Article

Keratins are asymmetrically inherited fate determinants in the mammalian embryo

https://doi.org/10.1038/s41586-020-2647-4

Received: 23 October 2019

Accepted: 30 July 2020

Published online: 26 August 2020

Check for updates

Hui Yi Grace Lim[1], Yanina D. Alvarez[1], Maxime Gasnier[1], Yiming Wang[2], Piotr Tetlak[1], Stephanie Bissiere[1], Hongmei Wang[2], Maté Biro[3] & Nicolas Plachta[1,4]✉

To implant in the uterus, the mammalian embryo first specifies two cell lineages: the pluripotent inner cell mass that forms the fetus, and the outer trophectoderm layer that forms the placenta[1]. In many organisms, asymmetrically inherited fate determinants drive lineage specification[2], but this is not thought to be the case during early mammalian development. Here we show that intermediate filaments assembled by keratins function as asymmetrically inherited fate determinants in the mammalian embryo. Unlike F-actin or microtubules, keratins are the first major components of the cytoskeleton that display prominent cell-to-cell variability, triggered by heterogeneities in the BAF chromatin-remodelling complex. Live-embryo imaging shows that keratins become asymmetrically inherited by outer daughter cells during cell division, where they stabilize the cortex to promote apical polarization and YAP-dependent expression of CDX2, thereby specifying the first trophectoderm cells of the embryo. Together, our data reveal a mechanism by which cell-to-cell heterogeneities that appear before the segregation of the trophectoderm and the inner cell mass influence lineage fate, via differential keratin regulation, and identify an early function for intermediate filaments in development.

The development of multicellular organisms requires the specification of diverse lineages from a small group of cells within the embryo. During mammalian development, the first lineage segregation produces the pluripotent inner cell mass (ICM), which forms the fetus and primitive endoderm, and the outer trophectoderm that forms the placenta[1]. How these lineages are specified remains unclear. The 'inside–outside' model suggests that lineage fates are specified by local signals after cells segregate into inner-outer positions[3]. Contrary to this model, heterogeneities in histone modifications[4], transcription factor dynamics[5], non-coding RNA localization[6], and gene expression[7–10] appearing as early as the four-cell stage bias the acquisition of pluripotent and trophectoderm fates, yet the mechanism is unclear.

By contrast, the 'cell polarity' model proposes that asymmetric inheritance of polarity components during cell division specifies distinct fates[11]. Some suggested that this relies on the asymmetric inheritance of the apical domain, which forms at the eight-cell stage before divisions segregating inner and outer cells, via enrichment of F-actin, PAR6 and aPKC at the apical cortex[12–14]. This would be consistent with studies showing that apical polarity at later stages promotes nuclear retention of the transcription factor YAP, which supports high expression of CDX2, a key transcription factor that specifies trophectoderm identity[15]. However, live-embryo imaging revealed that the apical domain disassembles from the cortex before division, instead of being directly inherited[16]. Therefore, it remains unclear whether other polarized components function as asymmetrically inherited fate determinants during mammalian development, similar to those in non-mammalian embryos[2], and how they relate to heterogeneities at earlier stages.

The cytoskeleton is not only composed of F-actin and microtubules, but also of various intermediate filaments[17]. During preimplantation development, keratins are the only cytoplasmic intermediate filaments that are expressed[18–20]. Keratins regulate polarity, signalling and mechanics in epithelial tissues[17], and have traditionally served as markers of trophectoderm[19]. Moreover, keratin knockouts display trophoblast fragility, placental bleeding and lethality after implantation[21–23]. Yet, keratin functions during preimplantation development remain unknown.

To study their functions, we performed immunofluorescence for keratins 8 and 18 (K8 and K18), the subtypes that are predominantly expressed during preimplantation stages[24]. In contrast to F-actin and microtubules, keratins are the first cytoskeletal component that displays cell-to-cell variability during development[25,26] (Fig. 1a). Although keratins are well-established markers of trophectoderm, the first filaments are already detected in a subset of cells of the eight-cell mouse embryo, before lineage segregation, with a similar pattern in the human embryo (Fig. 1, Extended Data Fig. 1a–c). The proportion of cells assembling filaments increases over time (Fig. 1b–d), and by the blastocyst stage the trophectoderm is covered by a dense network, whereas the ICM is devoid of keratins[18,27] (Fig. 1b–c, Extended Data Fig. 1d, Supplementary Video 1). Thus, variability in the assembly of keratin filaments establishes differences in cytoskeletal organization before segregation of the ICM and trophectoderm.

[1]Institute of Molecular and Cell Biology, ASTAR, Singapore, Singapore. [2]State Key Laboratory of Stem Cell and Reproductive Biology, Institute of Zoology, Chinese Academy of Science, Beijing, China. [3]EMBL Australia, Single Molecule Science Node, School of Medical Sciences, University of New South Wales, Sydney, New South Wales, Australia. [4]Department of Cell and Developmental Biology and Institute for Regenerative Medicine, Perelman School of Medicine, University of Pennsylvania, Philadelphia, PA, USA. ✉e-mail: plachtalab@gmail.com

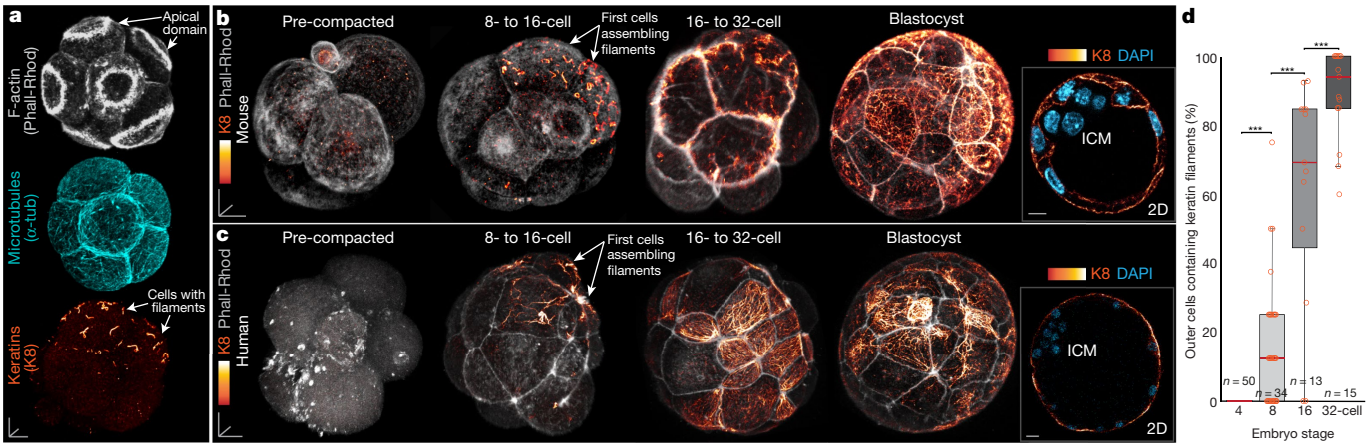

Fig. 1 | Keratin filaments display cell-to-cell variability before lineage segregation in the mouse and human embryo. a, All cells of the 8-cell embryo show similar F-actin and microtubule organization, yet only a subset assembles keratin filaments. Data are from five independent experiments. **b**, **c**, Mouse and human embryos at several developmental stages. Keratin filaments initially assemble in a subset of cells at the 8- to 16-cell stage, before inner–outer cell segregation. Blastocysts show dense keratin networks in the trophectoderm, but not in the ICM. Insets show middle 2D views. **d**, Quantification of keratin filament-forming outer cells of the embryo throughout preimplantation development. In box plots, the centre line is the median, box edges show upper and lower quartiles and whiskers represent the range. ***$P < 0.0001$, analysis of variance (ANOVA) test. Data are from three independent experiments. Scale bars, 10 µm.

We next microinjected embryos with mRNA for fluorescently labelled K18 (K18-Emerald), which display expression patterns that resemble endogenous keratins (Extended Data Fig. 1e–g). Live-imaging and immunofluorescence show that keratin filaments start to assemble in the sub-cortical and cortical regions during interphase, before apical domain formation (Extended Data Fig. 2a, b, Supplementary Video 2). The size of keratin filaments increases over time, and their motion is unconfined with an average speed of 0.45 ± 0.08 µm min^{-1} (Extended Data Fig. 2c–f), similar to measurements in cultured cells[28]. However, when the apical domain forms, keratins become more static and enriched at this structure, which suggests that keratins anchor to the apical domain (Fig. 2a, Extended Data Fig. 2a–b, f–g, Supplementary Video 3). Consistently, treatment with cytochalasin D blocks the formation of apical domains and shifts keratin localization to more uniform along the cortex and cytoplasm (Fig. 2a, Extended Data Fig. 2h). By contrast, acute treatment with SiR-Actin, which stabilizes F-actin, increases the density of F-actin at the apical domain and keratin apical polarization (Fig. 2a, Extended Data Fig. 2h). Therefore, the apical domain serves as scaffold to enrich keratins apically during interphase.

In many tissues, keratins anchor to the cortex via desmosomes[17]. Although mature desmosomes assemble by blastocyst stage, desmosome components are expressed in eight-cell embryos[29,30]. Immunofluorescence for the endogenous desmosome components plakoglobin, plakophilin and desmoglein2 reveals their localization to the apical domain (Extended Data Fig. 3a–c). Imaging fluorescently labelled desmoglein2 and K18 in live embryos confirms this pattern (Extended Data Fig. 3d–f). Furthermore, downregulation of desmosome proteins reduces keratin apical polarization (Extended Data Fig. 3g, h). Thus, desmosome components link keratin filaments to the apical domain.

When cells enter mitosis, they largely disassemble their apical domain[16], cortical microtubules, and desmosome components (Extended Data Figs. 3e, 4a). By contrast, keratins are stably retained within mitotic cells across different developmental stages, consistent with fluorescence recovery after photobleaching (FRAP) revealing a larger immobile fraction for keratins than actin (Extended Data Fig. 4b–d). Notably, live imaging of embryos expressing K18-Emerald shows that keratin filaments become asymmetrically inherited by the outer daughter cell during divisions producing inner–outer daughters, and symmetrically inherited during divisions producing outer–outer cells (Fig. 2b, Extended Data Fig. 4e, f, Supplementary Video 4). We confirmed these inheritance patterns in non-injected embryos (Extended Data Fig. 5a). These findings establish keratins as an asymmetrically inherited component during cell division.

To explore the inheritance mechanism, we used short interfering RNAs (siRNAs) that target PARD6B, which prevent the formation of the apical domain without interfering with the completion of mitosis[16,31] (Extended Data Fig. 5b). Knockdown of PARD6B reduces keratin apical polarization in interphase (Fig. 2a) and causes a more symmetric inheritance, even during divisions producing inner–outer daughter cells (Fig. 2c), which indicates that apical polarization of keratins before division is required for their asymmetric inheritance. Tracking keratins throughout mitosis shows that they still retain a high apical polarization, even after apical domain disassembly (Extended Data Fig. 2a, f), which was confirmed via immunofluorescence and in human embryos (Extended Data Fig. 5a, c). This apical retention suggests that some property of the cell hinders keratin movement, as long polymers diffuse more slowly through dense entangled meshworks[32]. Consistently, we found that mitotic cells display a dense cytoplasmic F-actin meshwork similar to earlier stages[33], through which keratin filaments move (at 0.4 µm min^{-1}) (Fig. 2d, Extended Data Fig. 5d, e). The speed of keratin filaments is inversely proportional to their volume (Extended Data Fig. 5f), in line with polymer studies[34]. Disrupting the F-actin meshwork using cytochalasin D specifically during mitosis causes keratins to move faster and lose their apical localization (Extended Data Fig. 5g). Moreover, when cells are arrested in metaphase using MG132, keratins have a longer time to move through the F-actin meshwork and eventually lose their apical localization (Extended Data Fig. 5g). As the distance between the apical cortex and cytokinetic furrow is 23.5 ± 1.52 µm (mean ± s.d.), and the time between apical domain disassembly and cytokinesis is 34.9 ± 6.2 min (Extended Data Fig. 5h), our results indicate that the slow movement of keratins through the dense F-actin meshwork during the relatively short duration of mitosis biases their apical retention. Hence, we propose a mechanism for keratin inheritance in which (1) the apical domain provides a scaffold promoting apical localization of keratins during interphase via desmosome proteins, and (2) after disassembly of this scaffold in mitosis, the cytoplasmic meshwork of F-actin hinders keratin movement, maintaining most filaments apically and biasing their inheritance by the outer cell.

Given their asymmetric inheritance by outer cells, we explored whether keratins influence trophectoderm specification. Analysis of

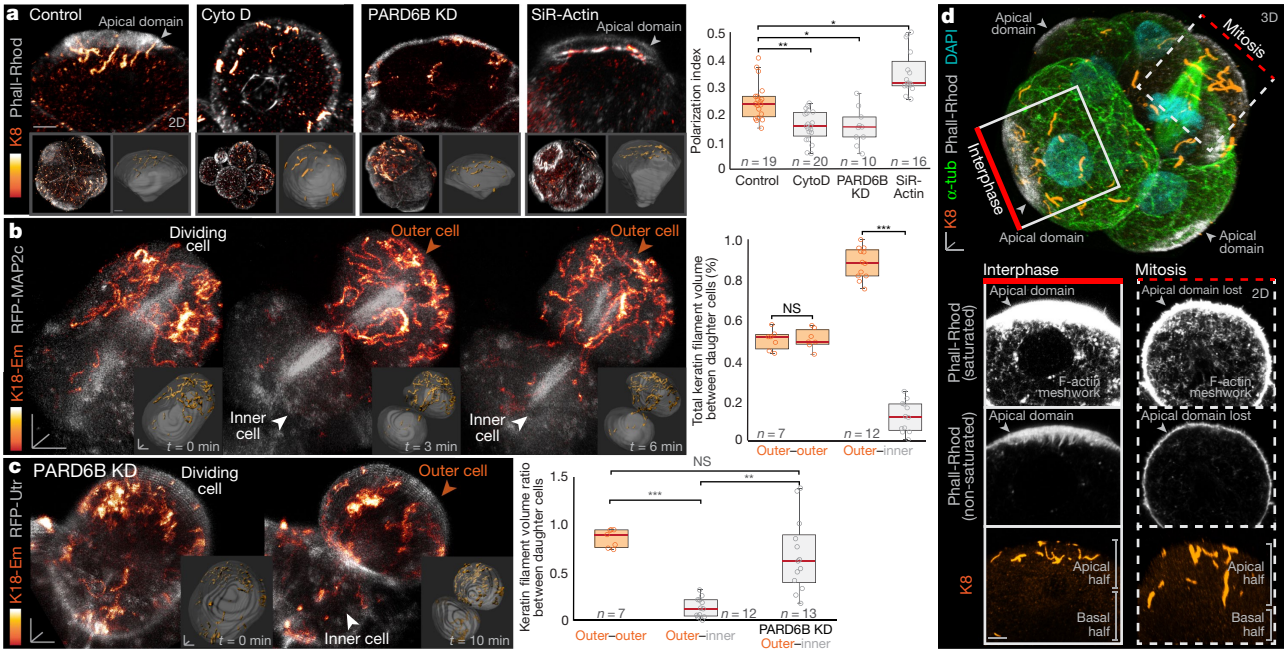

Fig. 2 | Keratin filaments are asymmetrically inherited during cell division. **a**, Keratin filaments are apically localized near the apical domain. Treatment with cytochalasin D and PARD6B knockdown (KD) reduce apical localization of keratins, whereas SiR-Actin increases it. Top panels show individual cells. Bottom panels show whole embryo (left) and computationally rendered filaments within each cell (right). Phall-Rhod, phalloidin-rhodamine. $^{**}P = 0.004$; $^{*}P = 0.02$ for PARD6B KD; $^{*}P = 0.03$ for SiR-Actin; Kruskal–Wallis test. **b**, Imaging fluorescently tagged keratins within the live embryo reveals their asymmetric inheritance by the outer daughter during divisions producing inner and outer cells. Quantification shows inheritance patterns. RFP–MAP2c, red fluorescent protein (RFP)-tagged MAP2c. NS, not significant. $^{***}P < 0.0001$, Student's *t*-test. **c**, PARD6B knockdown shifts keratin inheritance from asymmetric to more symmetric in outer–inner divisions. $^{***}P = 0.0001$; $^{**}P = 0.0009$; Kruskal–Wallis test. **d**, Immunofluorescence of eight-cell embryo highlights cytoskeletal organization in interphase and mitosis. While the apical domain and cortical microtubules become largely reorganized during mitosis, keratins retain their apical localization. 2D panels show loss of apical domain, but retention of a dense cytoplasmic F-actin meshwork and apically-localized keratins during mitosis. Data are from five independent experiments. In box plots, the centre line is the median, box edges show upper and lower quartiles and whiskers represent the range. Scale bars, 5 µm.

8- to 16-cell embryos shows that after division, cells inheriting keratins rapidly establish a dense network under the cortex (Fig. 3a). Although most 16-cell outer blastomeres reform an apical F-actin ring after division[16], only those that inherit keratins display higher levels of the apical polarity proteins PARD6B and PKCζ (Fig. 3b), and a larger immobile fraction of mRuby2-actin at this ring, compared to keratin-negative cells (Extended Data Fig. 6a–c). Furthermore, manipulation of actin stability per se using cytochalasin D reduces polarization, whereas stabilization with SiR-Actin increases polarization (Extended Data Fig. 6d). Knockdown of desmosome components also reduces actin stability (Extended Data Fig. 6a–c) and disrupts polarity (Extended Data Fig. 6e). Thus, keratins promote apical polarization by regulating the stability of F-actin.

Apical polarization is thought to oppose cell internalization and trigger YAP-dependent expression of CDX2 to establish trophectoderm identity[12,13]. Consistently, keratin-inheriting cells remain restricted to the outer layer, whereas most keratin-negative cells can undergo apical constriction[35] to form the ICM (Extended Data Fig. 6f, g, Supplementary Video 5). Keratin-inheriting cells also display the highest levels of nuclear YAP and CDX2, and the lowest levels of NANOG (Fig. 3b, c). Consistently, apical AMOT, which links apical polarity to YAP localization[36,37], is also enriched in these cells (Extended Data Fig. 6h). To test the role of keratins in trophectoderm specification, we combined siRNAs for K8 and K18, an approach that minimizes compensatory effects from weakly expressed keratins[38] and extensively eliminates the keratin network (Extended Data Fig. 7a, b). In contrast to cells inheriting keratins, K8/K18-knockdown cells display lower levels of apical PARD6B, PKCζ and AMOT, reduced nuclear expression of YAP and CDX2, and higher expression of NANOG (Fig. 3b, c, Extended Data Fig. 6h). CDX2 and NANOG levels in these knockdown cells are similar to inner cells, suggesting that K8/K18-knockdown cells are not yet specified to the trophectoderm (Fig. 3b, c). By contrast, co-injecting a high concentration of *K8* (also known as *Krt8*) and *K18* (*Krt18*) mRNA triggers the formation of a premature keratin network across all cells (Extended Data Fig. 7c), accompanied by widespread increase in CDX2 expression (Fig. 3d). Although the inner cells of these embryos inherit some overexpressed keratins, they still display low nuclear YAP and CDX2 levels, consistent with their lack of apical polarity (Extended Data Fig. 7d, e). Furthermore, keratin-positive cells in YAP-knockdown embryos are unable to maintain CDX2 expression, confirming that keratins regulate CDX2 via YAP (Extended Data Fig. 7f). Finally, microinjecting a rescue keratin construct restores CDX2 levels in K8/K18-knockdown embryos (Extended Data Fig. 7g). Therefore, keratins control the specification of the first trophectoderm cells of the embryo.

By the blastocyst stage, cells that did not inherit keratins eventually assemble a dense keratin network (Fig. 1b–d, Extended Data Fig. 1d) and display apical polarity and trophectoderm markers (Fig. 3b). This coincides with the appearance of junctional desmosomes (Extended Data Fig. 8a) and embryo cavitation, a process that requires mechanical stability to support rising intercellular pressure[39]. Although K8/K18-knockdown embryos still cavitate and form a blastocyst, they exhibit decreased volume, higher junctional tortuosity, greater surface curvature indicative of lower apical tension, and reduced cytoplasmic stiffness, assessed by tracking the movement of cytoplasmic nanoparticles[40] (Extended Data Fig. 8b–e). These defects are reversed using rescue keratin constructs (Extended Data Fig. 8f). Thus, in addition to specifying the first trophectoderm cells, keratins subsequently confer mechanical support for blastocyst morphogenesis.

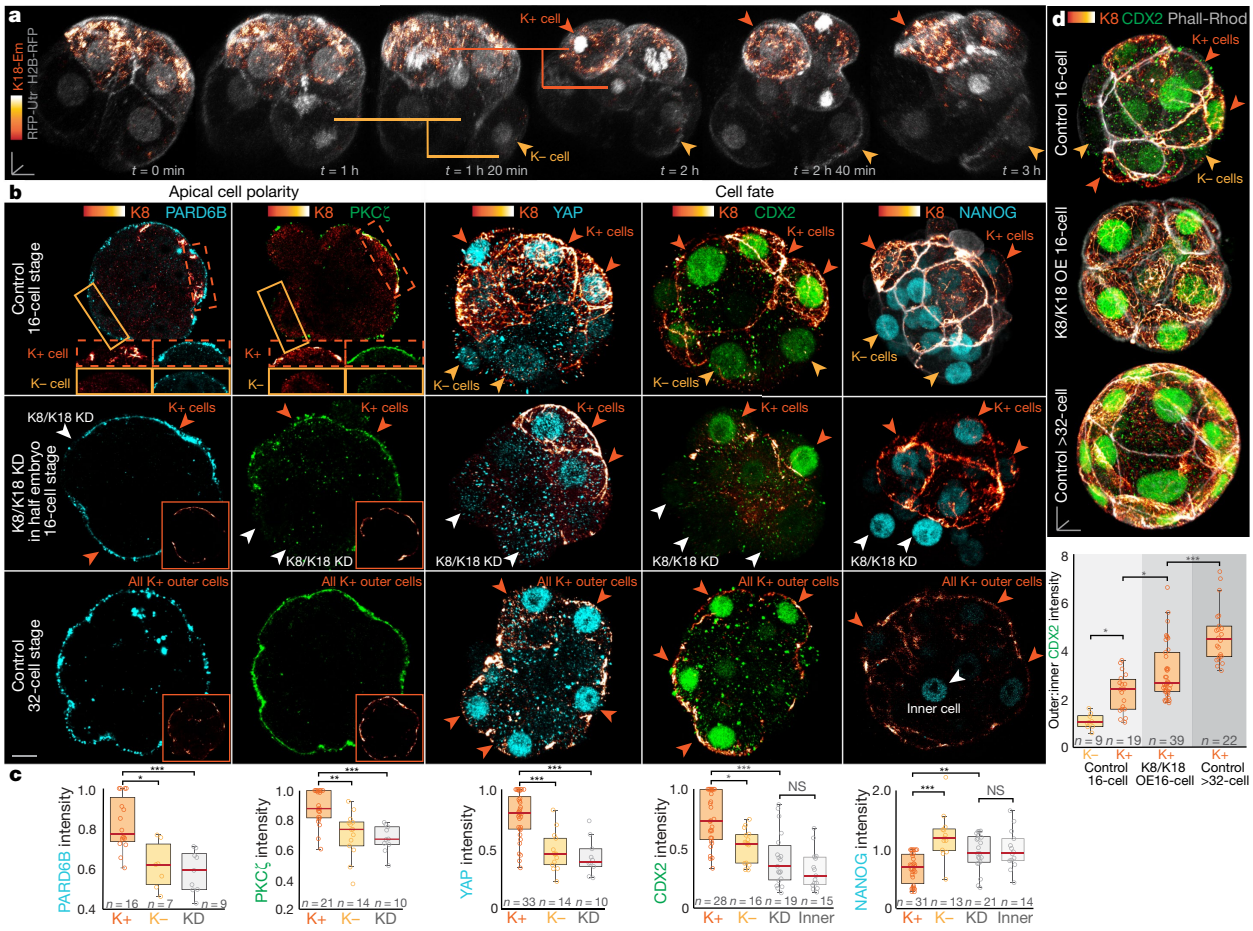

Fig. 3 | Keratin inheritance specifies the first trophectoderm cells of the embryo. a, Live-embryo imaging shows that outer cells inheriting keratins (K+) establish an extensive network after division, whereas those that did not remain devoid of filaments (K–). Data are from five independent experiments. **b**, Immunofluorescence in non-injected embryos shows that K+ cells are the first to display high levels of apical polarity and trophectoderm fate markers (top), but K8/K18-knockdown cells fail to establish these features (middle). By the 32-cell stage, the remaining cells of the embryo establish a keratin network and trophectoderm identity (bottom). Data are from three independent experiments. **c**, Quantification of fluorescence intensities. For PARD6B, $^{*}P = 0.01$; $^{***}P = 0.0006$. For PKCζ, $^{**}P = 0.001$; $^{***}P = 0.0002$. For YAP, $^{***}P < 0.0001$. For CDX2, $^{*}P = 0.01$; $^{***}P < 0.0001$. For NANOG, $^{***}P < 0.0001$; $^{**}P = 0.004$; Kruskal–Wallis test for PARD6B, PKCζ and CDX2; ANOVA test for YAP and NANOG. **d**, Keratin overexpression (K8/K18 OE) causes premature establishment of a keratin network and trophectoderm fate throughout the 16-cell embryo. $^{*}P = 0.03$ for control 16-cell; $^{*}P = 0.02$ for K8/K18 OE; $^{***}P < 0.0001$; ANOVA test. Data are from three independent experiments. In box plots, the centre line is the median, box edges show upper and lower quartiles and whiskers represent the range. Scale bars, 10 µm.

As keratins first appear in a subset of cells and function as fate determinants, they could link heterogeneities within the early embryo to lineage specification[1]. At the eight-cell stage, keratin-forming cells are connected by a microtubule bridge that links sister cells[41], indicating that they originate from the same four-cell blastomere (Fig. 4a, Extended Data Fig. 9a). Hence, we assessed whether they derive from the vegetal blastomere of the four-cell embryo (Extended Data Fig. 9b), shown to produce more trophectoderm than ICM progeny[4,42]. Selective photoactivation of the vegetal blastomere followed by staining for endogenous keratins at the eight-cell stage, and imaging live embryos expressing K18-Emerald during the four- to eight-cell window demonstrate that the vegetal blastomere preferentially produces keratin filament-forming cells (Fig. 4b, c, Extended Data Fig. 9c, d).

We finally focused on the BRG1-associated factor (BAF) chromatin remodelling complex, which promotes trophectoderm differentiation and is negatively regulated by the histone methyltransferase CARM1 that biases ICM fate[43,44]. The vegetal blastomere has the highest levels of BAF155, the main regulatory component of the BAF complex[43] (Fig. 4d). Higher BAF155 expression is also maintained in the first eight-cell blastomeres that assemble keratin filaments (Fig. 4e). Thus, we tested whether establishing four-cell embryos with different BAF patterns alters keratin expression at the eight-cell stage, by microinjecting *BAF155* (also known as *Smarcc1*) siRNAs or high levels of *BAF155* mRNA into one-cell embryos, or into one cell of two-cell embryos (Fig. 4f, Extended Data Fig. 9e). This generates patterns ranging from no detectable BAF155, to higher than normal BAF155 in all blastomeres. BAF155 knockdown or overexpression within all blastomeres triggers a reduction or increase in keratin expression, respectively. Consistently, when BAF155 levels are manipulated in half of the embryo, the resulting embryos display greater variability in keratin expression. To further determine how BAF155 regulates keratins, we used the transcriptional inhibitor actinomycin D, which eliminates keratin expression (Extended Data Fig. 9f). By contrast, facilitating transcription using trichostatin A elicits widespread keratin expression in most cells, and bypassing keratin transcription by microinjection of *K8* and *K18* mRNAs induces premature and extensive keratin expression (Extended Data Fig. 9f, g), which suggests that keratin expression is transcriptionally regulated. Furthermore, embryos that overexpress BAF155 no longer display high keratin levels when treated with actinomycin D (Extended Data Fig. 9h).

CARM1 methylates BAF155 at residue R1064[44] and CARM1-knockout embryos display lower levels of BAF155 methylation[43]. Consistently, the vegetal blastomere not only has the lowest CARM1[4] and highest total

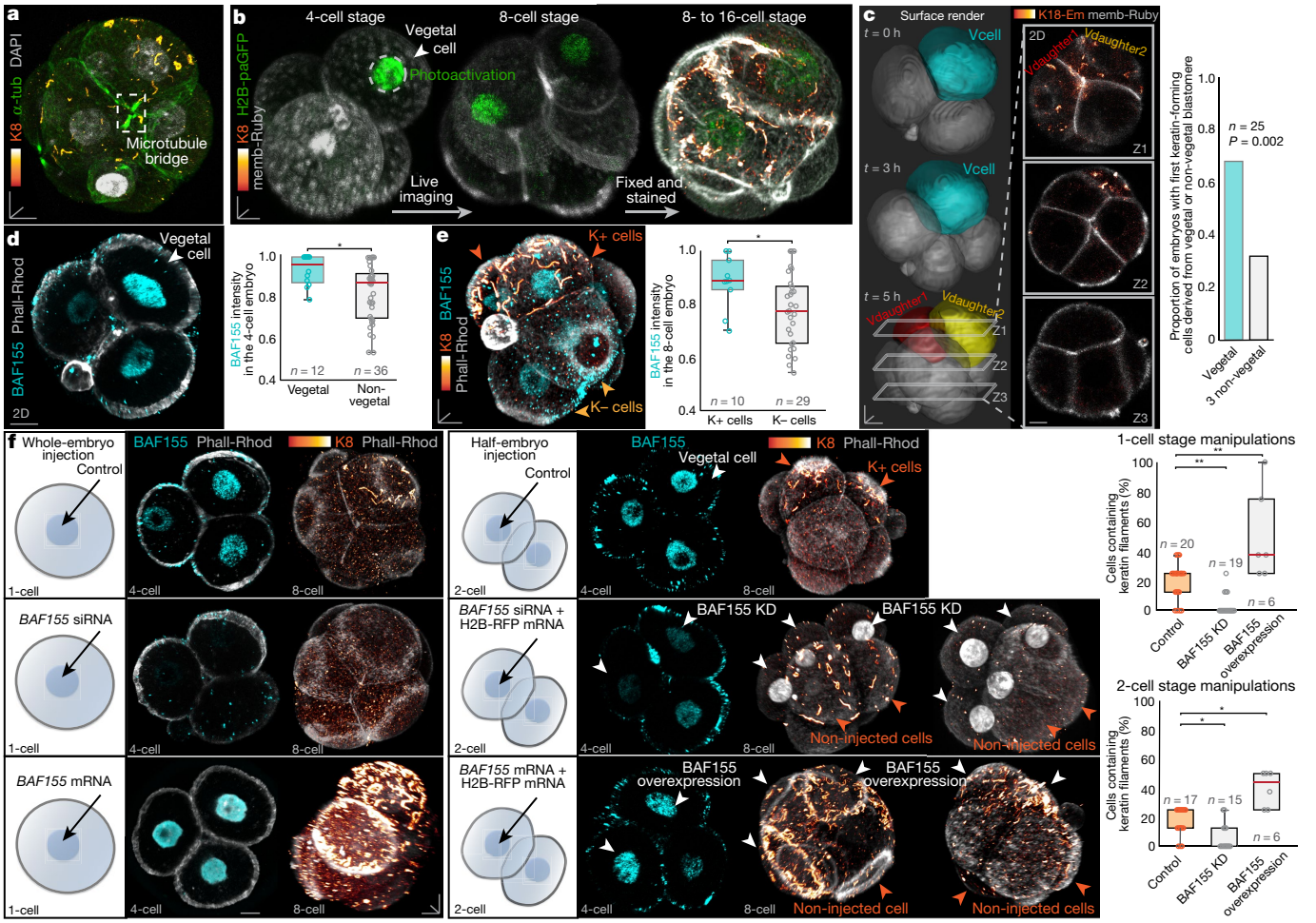

Fig. 4 | Keratin expression is regulated by early heterogeneities in the BAF complex. a, A microtubule bridge connecting sister cells reveals that the first eight-cell blastomeres assembling keratins originate from a common four-cell blastomere. Data are from three independent experiments. **b**, Selective H2B-paGFP photoactivation marks the vegetal blastomere that then produces the first keratin-forming cells. Data are from three independent experiments. **c**, Live-imaging of K18-Emerald during the four- to eight-cell stage confirms that the vegetal blastomere produces the first keratin-forming cells. *Z*-slices show keratin filaments in the cells derived from the vegetal blastomere. Graph shows proportion of embryos in which keratin-forming cells derive from vegetal blastomeres. $^{**}P = 0.002$, χ^2 test. **d**, The vegetal blastomere displays the highest endogenous BAF155 levels. $^{*}P = 0.01$; Mann–Whitney *U*-test. **e**, The first cells to form keratin filaments in the 8-cell embryo express higher BAF155 levels than cells without keratins. $^{*}P = 0.03$, Mann–Whitney *U*-test. **f**, Experimental manipulation of BAF155 levels produce different patterns of keratin expression. BAF155 knockdown reduces the proportion of cells expressing keratins at the eight-cell stage, whereas BAF155 overexpression can induce ectopic keratin expression. $^{*}P = 0.03$, $^{**}P = 0.005$ for KD; $^{**}P = 0.004$ for overexpression; ANOVA test for one-cell manipulations; Kruskal–Wallis test for two-cell manipulations. In box plots, the centre line is the median, box edges show upper and lower quartiles and whiskers represent the range. Scale bars, 10 µm.

BAF155 levels (Fig. 4d), but also the lowest levels of methylated BAF155 (Extended Data Fig. 9i). Overexpression of CARM1 disrupts keratin expression, similarly to BAF155 knockdown, and overexpression of a BAF155(R1064K) mutant that cannot be methylated by CARM1[44] causes premature keratin expression (Extended Data Fig. 9j–l). Finally, CDX2 expression is diminished in 16-cell embryos after BAF155 knockdown or CARM1 overexpression (Extended Data Fig. 9m, n). Thus, CARM1 methylation of BAF155 leads to the differential regulation of keratins.

In conclusion, keratins function as asymmetrically inherited factors that specify the first trophectoderm cells of the embryo (Extended Data Fig. 10). Our findings validate a key aspect of the 'cell polarity' model[11] by identifying keratins as an asymmetrically inherited fate determinant. Yet, they also highlight important distinctions by showing that eight-cell blastomeres are not equivalent. Although all cells initially display apical domains, only a subset expresses keratins. Therefore, even before inner–outer segregation, cells acquire differences in cytoskeletal organization biasing their fate. Moreover, differential expression of keratins is traced back to BAF heterogeneities within the four-cell embryo, providing a mechanism to understand how early cell-to-cell variability is transmitted through divisions to influence lineage fate. This extends the idea that the fate of early blastomeres is predictable[4–6,8,10,43,45–47].

Our study also reveals interactions between the actin cortex and keratins that are important for trophectoderm specification. The apical domain first promotes apical enrichment of keratins, but after division, keratins stabilize the cortex to prevent cell internalization, support apical polarization and promote acquisition of the first hallmarks of trophectoderm specification. At later stages, CDX2 was shown to promote keratin expression[27]. Thus, the initial effect of keratins in promoting CDX2 expression could feedback into the production of more keratins to support the expansion of the keratin network for blastocyst morphogenesis. Finally, the comparable cell-to-cell variability and localization of keratins in the human embryo suggest that keratin asymmetric inheritance may represent a conserved mechanism of lineage specification in early mammalian development.

Online content

Any methods, additional references, Nature Research reporting summaries, source data, extended data, supplementary information, acknowledgements, peer review information; details of author contributions and competing interests; and statements of data and code availability are available at https://doi.org/10.1038/s41586-020-2647-4.

1. White, M. D., Zenker, J., Bissiere, S. & Plachta, N. Instructions for assembling the early mammalian embryo. *Dev. Cell* **45**, 667–679 (2018).
2. Knoblich, J. A. Asymmetric cell division: recent developments and their implications for tumour biology. *Nat. Rev. Mol. Cell Biol.* **11**, 849–860 (2010).
3. Tarkowski, A. K. & Wróblewska, J. Development of blastomeres of mouse eggs isolated at the 4- and 8-cell stage. *J. Embryol. Exp. Morphol.* **18**, 155–180 (1967).
4. Torres-Padilla, M. E., Parfitt, D. E., Kouzarides, T. & Zernicka-Goetz, M. Histone arginine methylation regulates pluripotency in the early mouse embryo. *Nature* **445**, 214–218 (2007).
5. White, M. D. et al. Long-lived binding of Sox2 to DNA predicts cell fate in the four-cell mouse embryo. *Cell* **165**, 75–87 (2016).
6. Wang, J. et al. Asymmetric expression of LincGET biases cell fate in two-cell mouse embryos. *Cell* **175**, 1887–1901.e18 (2018).
7. Biase, F. H., Cao, X. & Zhong, S. Cell fate inclination within 2-cell and 4-cell mouse embryos revealed by single-cell RNA sequencing. *Genome Res.* **24**, 1787–1796 (2014).
8. Goolam, M. et al. Heterogeneity in Oct4 and Sox2 targets biases cell fate in 4-cell mouse rmbryos. *Cell* **165**, 61–74 (2016).
9. Shi, J. et al. Dynamic transcriptional symmetry-breaking in pre-implantation mammalian embryo development revealed by single-cell RNA-seq. *Development* **142**, 3468–3477 (2015).
10. Casser, E. et al. Totipotency segregates between the sister blastomeres of two-cell stage mouse embryos. *Sci. Rep.* **7**, 8299 (2017).
11. Johnson, M. H. & Ziomek, C. A. The foundation of two distinct cell lineages within the mouse morula. *Cell* **24**, 71–80 (1981).
12. Maître, J. L. et al. Asymmetric division of contractile domains couples cell positioning and fate specification. *Nature* **536**, 344–348 (2016).
13. Anani, S., Bhat, S., Honma-Yamanaka, N., Krawchuk, D. & Yamanaka, Y. Initiation of Hippo signaling is linked to polarity rather than to cell position in the pre-implantation mouse embryo. *Development* **141**, 2813–2824 (2014).
14. Korotkevich, E. et al. The Apical domain is required and sufficient for the first lineage segregation in the mouse embryo. *Dev. Cell* **40**, 235–247.e7 (2017).
15. Nishioka, N. et al. The Hippo signaling pathway components Lats and Yap pattern Tead4 activity to distinguish mouse trophectoderm from inner cell mass. *Dev. Cell* **16**, 398–410 (2009).
16. Zenker, J. et al. Expanding actin rings zipper the mouse embryo for blastocyst formation. *Cell* **173**, 776–791.e17 (2018).
17. Coulombe, P. A. & Wong, P. Cytoplasmic intermediate filaments revealed as dynamic and multipurpose scaffolds. *Nat. Cell Biol.* **6**, 699–706 (2004).
18. Jackson, B. W. et al. Formation of cytoskeletal elements during mouse embryogenesis. Intermediate filaments of the cytokeratin type and desmosomes in preimplantation embryos. *Differentiation* **17**, 161–179 (1980).
19. Paulin, D., Babinet, C., Weber, K. & Osborn, M. Antibodies as probes of cellular differentiation and cytoskeletal organization in the mouse blastocyst. *Exp. Cell Res.* **130**, 297–304 (1980).
20. Oshima, R. G., Howe, W. E., Klier, F. G., Adamson, E. D. & Shevinsky, L. H. Intermediate filament protein synthesis in preimplantation murine embryos. *Dev. Biol.* **99**, 447–455 (1983).
21. Hesse, M., Franz, T., Tamai, Y., Taketo, M. M. & Magin, T. M. Targeted deletion of keratins 18 and 19 leads to trophoblast fragility and early embryonic lethality. *EMBO J.* **19**, 5060–5070 (2000).
22. Tamai, Y. et al. Cytokeratins 8 and 19 in the mouse placental development. *J. Cell Biol.* **151**, 563–572 (2000).
23. Baribault, H., Price, J., Miyai, K. & Oshima, R. G. Mid-gestational lethality in mice lacking keratin 8. *Genes Dev.* **7** (7A), 1191–1202 (1993).
24. Lu, H., Hesse, M., Peters, B. & Magin, T. M. Type II keratins precede type I keratins during early embryonic development. *Eur. J. Cell Biol.* **84**, 709–718 (2005).
25. Chisholm, J. C. & Houliston, E. Cytokeratin filament assembly in the preimplantation mouse embryo. *Development* **101**, 565–582 (1987).
26. Emerson, J. A. Disruption of the cytokeratin filament network in the preimplantation mouse embryo. *Development* **104**, 219–234 (1988).
27. Ralston, A. & Rossant, J. Cdx2 acts downstream of cell polarization to cell-autonomously promote trophectoderm fate in the early mouse embryo. *Dev. Biol.* **313**, 614–629 (2008).
28. Yoon, K. H. et al. Insights into the dynamic properties of keratin intermediate filaments in living epithelial cells. *J. Cell Biol.* **153**, 503–516 (2001).
29. Fleming, T. P., Garrod, D. R. & Elsmore, A. J. Desmosome biogenesis in the mouse preimplantation embryo. *Development* **112**, 527–539 (1991).
30. Den, Z., Cheng, X., Merched-Sauvage, M. & Koch, P. J. Desmocollin 3 is required for pre-implantation development of the mouse embryo. *J. Cell Sci.* **119**, 482–489 (2006).
31. Alarcon, V. B. Cell polarity regulator PARD6B is essential for trophectoderm formation in the preimplantation mouse embryo. *Biol. Reprod.* **83**, 347–358 (2010).
32. Doi, M. & Edwards, S. F. *The Theory of Polymer Dynamics* Vol. 73 (Oxford Univ, Press, 1988).
33. Almonacid, M., Terret, M. É. & Verlhac, M. H. Actin-based spindle positioning: new insights from female gametes. *J. Cell Sci.* **127**, 477–483 (2014).
34. Käs, J., Strey, H. & Sackmann, E. Direct imaging of reptation for semiflexible actin filaments. *Nature* **368**, 226–229 (1994).
35. Samarage, C. R. et al. Cortical tension allocates the first inner cells of the mammalian embryo. *Dev. Cell* **34**, 435–447 (2015).
36. Hirate, Y. et al. Polarity-dependent distribution of angiomotin localizes Hippo signaling in preimplantation embryos. *Curr. Biol.* **23**, 1181–1194 (2013).
37. Leung, C. Y. & Zernicka-Goetz, M. Angiomotin prevents pluripotent lineage differentiation in mouse embryos via Hippo pathway-dependent and -independent mechanisms. *Nat. Commun.* **4**, 2251 (2013).
38. Magin, T. M. et al. Lessons from keratin 18 knockout mice: formation of novel keratin filaments, secondary loss of keratin 7 and accumulation of liver-specific keratin 8-positive aggregates. *J. Cell Biol.* **140**, 1441–1451 (1998).
39. Leonavicius, K. et al. Mechanics of mouse blastocyst hatching revealed by a hydrogel-based microdeformation assay. *Proc. Natl Acad. Sci. USA* **115**, 10375–10380 (2018).
40. Wirtz, D. Particle-tracking microrheology of living cells: principles and applications. *Annu. Rev. Biophys.* **38**, 301–326 (2009).
41. Zenker, J. et al. A microtubule-organizing center directing intracellular transport in the early mouse embryo. *Science* **357**, 925–928 (2017).
42. Piotrowska-Nitsche, K., Perea-Gomez, A., Haraguchi, S. & Zernicka-Goetz, M. Four-cell stage mouse blastomeres have different developmental properties. *Development* **132**, 479–490 (2005).
43. Panamarova, M. et al. The BAF chromatin remodelling complex is an epigenetic regulator of lineage specification in the early mouse embryo. *Development* **143**, 1271–1283 (2016).
44. Wang, L. et al. CARM1 methylates chromatin remodeling factor BAF155 to enhance tumor progression and metastasis. *Cancer Cell* **30**, 179–180 (2016).
45. Plachta, N., Bollenbach, T., Pease, S., Fraser, S. E. & Pantazis, P. Oct4 kinetics predict cell lineage patterning in the early mammalian embryo. *Nat. Cell Biol.* **13**, 117–123 (2011).
46. Kaur, G. et al. Probing transcription factor diffusion dynamics in the living mammalian embryo with photoactivatable fluorescence correlation spectroscopy. *Nat. Commun.* **4**, 1637 (2013).
47. Tabansky, I. et al. Developmental bias in cleavage-stage mouse blastomeres. *Curr. Biol.* **23**, 21–31 (2013).

Methods

Mouse embryo work

Mouse embryo experimentation was approved by the Biological Resource Center Institutional Animal Care and Use Committee (IACUC), Agency for Science, Technology and Research (IACUC Protocol 181370). C57BL/6 wild-type 3–4-week-old female mice were superovulated using 5 IU of pregnant mare serum (PMS, National Hormone and Peptide Program) gonadotropin given intraperitoneally and 5 IU of recombinant chorionic gonadotrophin (CG, National Hormone and Peptide Program) given 48 h after and immediately before mating, according to animal ethics guidelines of the Agency for Science, Technology and Research, Singapore. Embryos were flushed from oviducts of plugged females using M2 medium (Merck) and cultured in KSOM+AA (Merck) covered by mineral oil (Sigma), at 37 °C and 5% CO_2. Microinjections were performed using a FemtoJet (Eppendorf). mRNA synthesis was performed on linearized plasmids using the mMESSAGE mMACHINE SP6 kit (Ambion), and purified using the RNAeasy kit (QIAGEN). For live imaging experiments, mRNAs diluted in injection buffer (5 mM Tris, 5 mM NaCl, 0.1 mM EDTA) were microinjected as follows: K8-Emerald and K18-Emerald at 150 ng μl^{-1}; mRuby2-Actin at 100 ng μl^{-1}; RFP-Utrophin at 70 ng μl^{-1}; RFP-MAP2c at 80 ng ul^{-1}; memb-mRuby2 at 70 ng μl^{-1}; H2B-RFP and H2B-GFP at 5 ng μl^{-1}; Desmoglein2-Emerald and Desmoglein2-mRuby2 at 150 ng μl^{-1}; H2B-paGFP at 20 ng ul^{-1}. For overexpression experiments, mRNAs were microinjected as follows: K8 and K18 at 300 ng μl^{-1}; BAF155 and BAF155(R1064K) at 500 ng μl^{-1}; CARM1 at 300 ng μl^{-1}. siRNAs (QIAGEN) were microinjected at the following concentrations: K8 (500 nM), K18 (500 nM), DSG2 (200 nM), DSC3 (200 nM), desmoplakin (200 nM), plakoglobin (200 nM), PARD6B (200 nM), YAP1 (200 nM), BAF155 (500 nM).

The siRNAs used are: Mm_Krt2-8_1 (AACCATGTACCAGATTAAG TA), Mm_Krt2-8_2 (ATGGATGGCATCATCGCTGAA), Mm_Krt1-18_1 (CAGAGTGGTGTCCGAGACTAA), Mm_Krt1-18_3 (CCGGGAACATCTGGAG AAGAA), Mm_Dsg2_1 (CAGCATTATGCCAATGAAGAA), Mm_Dsg2_2 (CTCC GTCACTTCAGAGATTAA), Mm_Dsc3_2 (CAGAGATAATTCAAGATTATA), Mm_Dsc3_5 (AACTGCGGATGTTCAAATATA), Mm_Dsp_2 (CAGGAAGTT CTTCGATCAATA), Mm_Dsp_4 (ACCGGTTGACATGGCGTATAA), Mm_ Jup_4 (CAGACAGTACACACTCAAGAA), Mm_Jup_5 (CACTATGGCTAT GGCCACTAA), Mm_Pard6b_3 (CACGGGCCTGCTAGCTGTCAA), Mm_Pard6b_4 (CAGGTGACTGACATGATGATA), Mm_Yap1_6 (ACCCTT GAACATATACATTTA), Mm_Yap1_7 (AACATCCTATTTAAATCTTAA), Mm_ Smarcc1_5 (ACGCATCCTGGTTTGATTATA), Mm_Smarcc1_6 (TCGAACTG ACATTTACTCCAA).

For drug treatments, all drugs were diluted in KSOM to the following concentrations: cytochalasin D at 20 µg ml^{-1}, SiR-Actin at 100 nM, MG-132 at 25 µM, actinomycin D at 100 ng ml^{-1}, trichostatin A at 75 nM. Drugs were applied for 2 h before embryo fixation, with the exception of actinomycin D and trichostatin A, which were both applied for the entire 4- to 8-cell stage window to effectively block or promote transcription respectively.

Human embryo work

Human embryos were donated to the Reproductive Medicine Research Center, Sixth Affiliated Hospital of Sun Yat-sen University for research purposes, following ethical guidelines of the Sixth Affiliated Hospital of Sun Yat-sen University. Experiments were performed according to the guidelines of the Institute of Zoology, Chinese Academy of Sciences and the Sixth Affiliated Hospital of Sun Yat-sen University.

This work was approved by the Ethics Committee of Center for Reproductive Medicine, Sixth Affiliated Hospital of Sun Yat-Sen University (Research license 2019SZZX-008). The Medicine Ethics Committee of Center for Reproductive Medicine, Sixth Affiliated Hospital of Sun Yat-Sen University is composed of 11 members, including experts of laws, scientists and clinicians with relevant expertise. The Committee evaluated the scientific merit and ethical justification of this study and conducted a full review of the donations and use of these samples.

All embryo donor couples signed informed consent forms for voluntary donations of surplus embryos for research, at the Center for Reproductive Medicine, Sixth Affiliated Hospital of Sun Yat-Sen University. Participation in the study was voluntary and no financial inducements were offered for embryo donation. The culture of all embryos was terminated before day 14 post-fertilization. Couples were informed that their embryos would be used to study the developmental mechanisms of human embryos and that their donation would not affect their IVF cycle. The informed consent forms clearly state the goals of the research, clinical procedures used in the study, potential benefits and risks to research participants, and steps taken to ensure that the privacy of each embryo donor was well protected. The participation of embryo donors in the study can only be obtained if eligible participants were provided with all necessary information about the study and the opportunity to receive counselling. These informed consent guidelines are in line with the ethical and regulatory framework set forth by the Center for Reproductive Medicine, Sixth Affiliated Hospital of Sun Yat-sen University, and complied with the International Society for Stem Cell Research (ISSCR) Guidelines for Stem Cell Research and Clinical Translation (2016) and Ethical Guidelines for Human Embryonic Stem Cell Research (2003) jointly issued by the Ministry of Science and Technology and the Ministry of Health of the People's Republic of China.

All donated samples in this study were obtained from frozen embryos from couples who signed informed consent agreements. The study employed standard clinical protocols for embryo collection, cryopreservation, thawing and culture procedures. Human embryos were frozen–thawed 3 or 5 days post-fertilization. Cryopreserved embryos were thawed using Kitazato Thawing Media Kit VT802 (Kitazato Dibimed) depending on the protocol used for freezing and following the manufacturer's instructions. The embryos were cultured in Single-step embryo culture medium (LifeGlobal) covered with oil (LifeGlobal) (from 4-cell stage to blastocyst stage). Embryos with normal morphology and cleavage patterns were used in this study.

Microscopy

Imaging was performed using a laser scanning confocal microscope (LSM 780 and LSM 880, Zeiss) with a water UV-VIS-IR Apochromat 63× 1.2 NA objective. For live imaging, embryos were cultured in LabTek chambers (Nunc) in KSOM+AA (Merck) covered by mineral oil (Sigma), using the incubator system adapted for the microscope (Carl Zeiss, Jena) to maintain the embryos at 37 °C and 5% CO_2. Embryos were scanned every 15 to 20 min for long-term imaging, and selected mitotic cells were imaged at higher temporal resolution of 1 to 3 min intervals in order to track the dynamics of keratin filaments throughout the entire cell division. FRAP was performed at 3.5-times zoom on a 5 µm × 10 µm region of interest, photobleached using the 488 nm laser at 100%, with a pixel dwell time of 6 µs and scanning speed of 6. For photoactivation experiments, H2B-paGFP was selectively illuminated in the nuclei of vegetal blastomeres using an 820 nm two-photon laser (Mai Tai, Spectra-Physics) as described[5,45], followed by live-imaging using a 488 nm laser to track the photoactivated signal in the daughter cells.

For measurements of cell elasticity, 0.1-µm-diameter carboxylate-modified FluoSpheres (Invitrogen) were microinjected into live embryos. The size of these nanoparticles is larger than the average mesh size of the cytoskeletal network[40]. We optimized their concentration to obtain an average of 10 beads per cell, homogenously distributed throughout the cytoplasm at blastocyst stage. Tracking of the movement of these nanoparticles was performed by imaging individual particles at 30-times zoom, 50 frames s^{-1} for 2 min, as previously described[48].

Immunofluorescence

Embryos were fixed in 4% paraformaldehyde for 30 min at room temperature or overnight at 4 °C, washed twice in PBS with 0.1% Triton X-100, permeabilized for 20 min in PBS with 0.5% Triton X-100, and incubated in PBS with 10% fetal bovine serum (blocking solution) for 30 min. Embryos were then incubated at 4 °C overnight in primary antibodies diluted in blocking solution, at the following concentrations: K8 (DSHB) at 1:20, K18 (Sigma, SAB4501665) at 1:200, K19 (DSHB) at 1:50, pan-Keratin (Cell Signaling, 4545) at 1:50, α-tubulin (Sigma, T6199) at 1:1,000, PARD6B (Santa Cruz, 166405) at 1:50, PKCζ (Santa Cruz, 17781) at 1:50, AMOT (gift from H. Sasaki) at 1:200, YAP (Cell Signaling, 8418S) at 1:500, CDX2 (Abcam, 88129) at 1:200, NANOG (Abcam, 80892) at 1:200, desmoglein1/2 (Progen, 61002S) undiluted, plakoglobin (Progen, 61005S) undiluted, plakophilin (Progen, 651101S) undiluted, desmoplakin1 (Progen) at 1:100, BAF155 (Santa Cruz, 48350) at 1:50, dimethyl-BAF155 (Merck, ABE1339) at 1:100, and CARM1 (Cell Signaling, 3379S) at 1:150. After primary antibody incubation, embryos were washed 5 times for 20 min in PBS with 0.1% Triton X-100 and incubated 1.5 h at room temperature or overnight at 4 °C in secondary antibodies diluted in blocking solution to 1:500. Phalloidin-Rhodamine (Molecular Probes, R415) diluted to 1:500 and NucBlue Fixed Cell Stain ReadyProbes reagent (Invitrogen) diluted to 1:100 in blocking solution were also used to label the F-actin and chromatin respectively. Embryos were washed three times in PBS with 0.1% Triton X-100 before mounting in PBS covered with mineral oil (Sigma) in an 8-well LabTek chamber (Nunc).

Image analysis

Image analyses were performed using Imaris 8.2 (Bitplane AG), Fiji, and MATLAB. 3D segmentation of whole embryos, individual cells and individual nuclei was performed using the Imaris manual surface rendering module, and 3D segmentation of keratin filaments was done with the automatic surface rendering mode. The Imaris statistics module was used to obtain values for total fluorescence intensities, cell volumes, and nucleus volumes. Measurements of apical fluorescence intensities of PARD6B and PKCζ were performed in Fiji by selecting the apical region of individual cells and averaging the fluorescence intensities across five different Z-planes. All quantifications were normalized to background fluorescence to correct for weaker fluorescence with increasing depth through the embryo. M.B. thanks Bitplane AG for an Imaris Developer License.

To quantify the localization of keratin filaments within individual cells, we used a polarization index, adapted from previous work[49,50]. Spatial coordinates for individual keratin filaments and the cell centre of mass, volumes of individual keratin filaments, and lengths of the cell apical-basal axis were obtained using Imaris software. The polarization index was calculated by obtaining the difference between the volume-weighted average position of all keratin filaments within the cell and the position of the cell centre of mass, normalized to the cell apical–basal axis.

For calculations of keratin filament movement during interphase and mitosis, the spatial coordinates of each filament were obtained from the Imaris statistics module. The mean speed of filament movement was calculated by dividing the distance between the initial and final positions of the filament by the elapsed time.

For analysis of FRAP experiments, mean fluorescence intensity at the photobleached region of interest (ROI) was corrected by background fluorescence and normalized to a non-photobleached reference. The average of the pre-bleach fluorescence intensities was set to 100%, and the fluorescence intensity immediately after photobleaching was set to 0%. The normalized mean fluorescence intensities were then fitted with an exponential function, as previously described[16]. The immobile fraction was calculated by taking $1 - I_\infty$, in which I_∞ is the normalized mean fluorescence intensity when the intensity recovers to a plateau. All fittings were performed in MATLAB, and FRAP kymographs were created using the Montage tool in Fiji.

To characterize the morphology of cell–cell junctions, we used a tortuosity index calculated by measuring the total junction length, normalized to the Euclidean distance.

For measurements of surface curvature, we first segmented individual cells in Imaris and extracted the apical surface of each cell using a custom MATLAB code. The radius of surface curvature was then determined using the radius of the sphere that best fits the cell apical surface.

Statistical analysis

Statistical analyses were performed in GraphPad Prism and Excel. Qualitative data were represented using a contingency table and analysed using a Fisher's exact test or χ^2 test. All quantitative data were first analysed for normality using a D'Agostino-Pearson omnibus normality test. Variables showing a normal distribution were then analysed using an unpaired, two-tailed Student's *t*-test or ANOVA with Tukey's multiple comparisons test for two groups or more than two groups respectively. Variables that did not show a normal distribution were analysed using an unpaired, two-tailed Mann–Whitney *U*-test or Kruskal–Wallis test with Dunn's multiple comparisons test for two groups or more than two groups respectively. No statistical test was performed to determine sample size, and sample size was determined based on previous experience and in accordance to previous studies. Embryos were randomly allocated into experimental groups and randomly selected for analysis. Reproducibility was confirmed by at least three independent experiments. The investigators were not blinded to allocation during experiments and outcome assessment.

Reporting summary

Further information on research design is available in the Nature Research Reporting Summary linked to this paper.

Data availability

Source data are provided with this paper.

Code availability

Code for apical surface curvature analysis has been published in a publicly available repository at https://github.com/gracelhy/Analysis-of-embryo-parameters.

48. Daniels, B. R., Masi, B. C. & Wirtz, D. Probing single-cell micromechanics in vivo: the microrheology of C. elegans developing embryos. *Biophys. J.* **90**, 4712–4719 (2006).
49. Park, H. Y., Trcek, T., Wells, A. L., Chao, J. A. & Singer, R. H. An unbiased analysis method to quantify mRNA localization reveals its correlation with cell motility. *Cell Rep.* **1**, 179–184 (2012).
50. Skamagki, M., Wicher, K. B., Jedrusik, A., Ganguly, S. & Zernicka-Goetz, M. Asymmetric localization of Cdx2 mRNA during the first cell-fate decision in early mouse development. *Cell Rep.* **3**, 442–457 (2013).

Acknowledgements We thank X. Liang for assistance with human embryo work. This work was supported by grants from ASTAR, EMBO, and HHMI to N.P., EMBL Australia to M.B., and the ASTAR Graduate Scholarship to H.Y.G.L.

Author contributions H.Y.G.L. conceived the project, performed the experiments and data analysis, and wrote the manuscript with contributions from all other authors. Y.D.A. and M.G. assisted with experiments and data analysis. Y.W. and H.W. performed human embryo studies. P.T. and S.B. performed mouse work and embryo microinjection experiments. M.B. contributed to data analysis and manuscript writing. N.P. supervised the project.

Competing interests The authors declare no competing interests.

Additional information

Supplementary information is available for this paper at https://doi.org/10.1038/s41586-020-2647-4.

Correspondence and requests for materials should be addressed to N.P.

Peer review information *Nature* thanks Magdalena Zernicka-Goetz and the other anonymous reviewer(s) for their contribution to the peer review of this work.

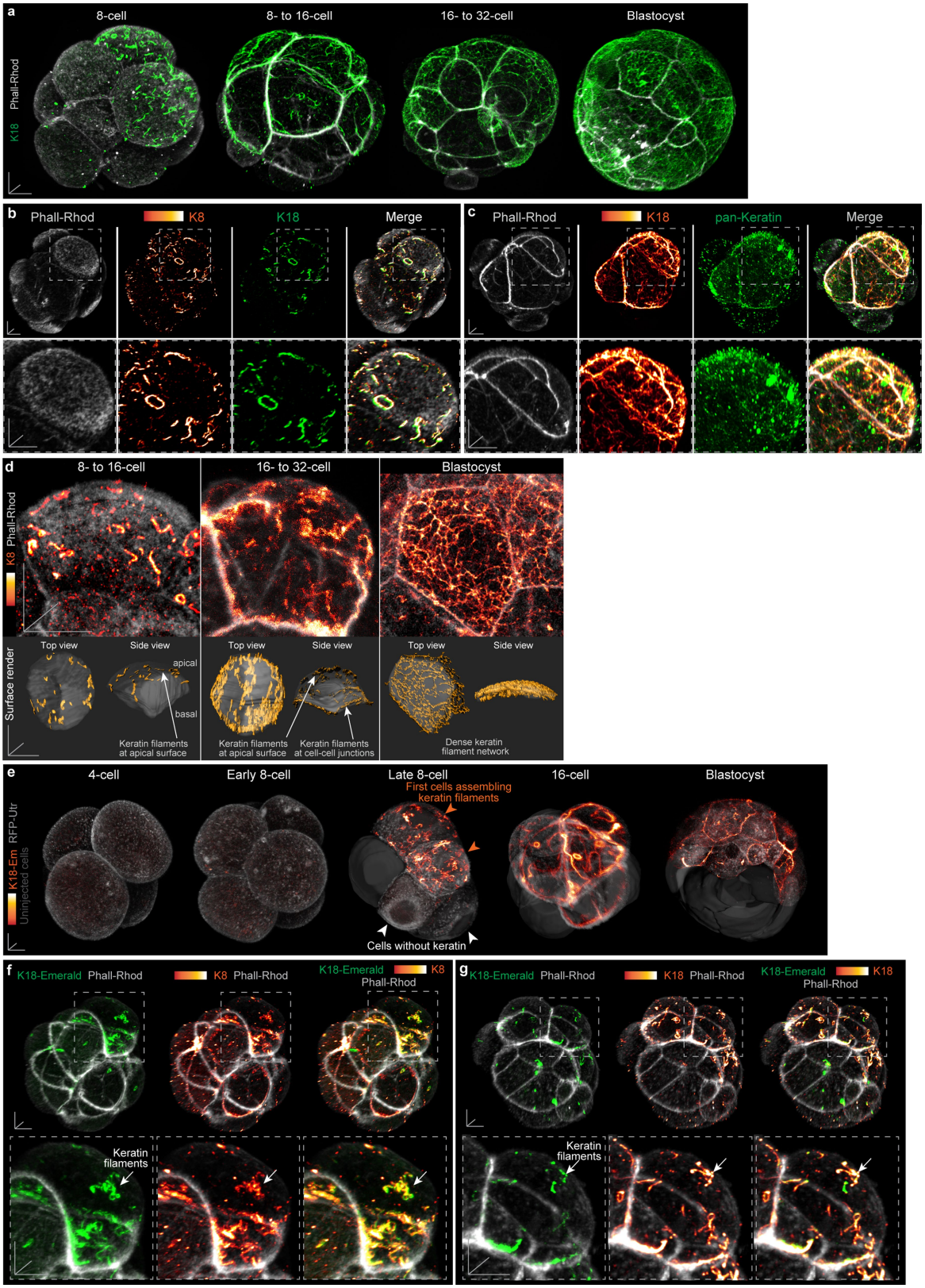

Extended Data Fig. 1 | See next page for caption.

Extended Data Fig. 1 | Keratin filaments in the preimplantation mouse embryo. a, 3D views of mouse embryos at multiple developmental stages, stained for K18. K18 expression and localization resemble that of K8. Note the initial assembly of filaments in a specific subset of cells in the 8-cell embryo. Data are from five independent experiments. **b**, Double immunofluorescence for K8 and K18 shows their colocalization in filament structures within the same embryo. Data are from three independent experiments. **c**, Double immunofluorescence using a pan-keratin antibody and K18 shows colocalization in filament structures within the same embryo. Data are from three independent experiments. **d**, High-magnification views highlight keratin filament organization at multiple developmental stages (top). Surface render of computationally-segmented cells and keratin filaments with top and side views show the changes in cell morphology and keratin filament organization at different developmental stages. The density of the keratin filament network increases over time and the filaments become enriched at cell-cell junctions. Data are from five independent experiments. **e**, Live imaging of embryos expressing K18-Emerald. A subset of cells begins to assemble keratin filaments at the eight-cell stage, similar to observations from immunofluorescence for endogenous keratins. No keratin filaments are detected in four-cell or early uncompacted eight-cell embryos. Data are from three independent experiments. **f**, **g**, Colocalization of K18-Emerald and immunofluorescence against K8 (**f**) or K18 (**g**). Bottom panels show zoomed views of single cells expressing keratin filaments, with arrows pointing to an example of signal colocalization. Data are from three independent experiments. Scale bars, 10 μm.

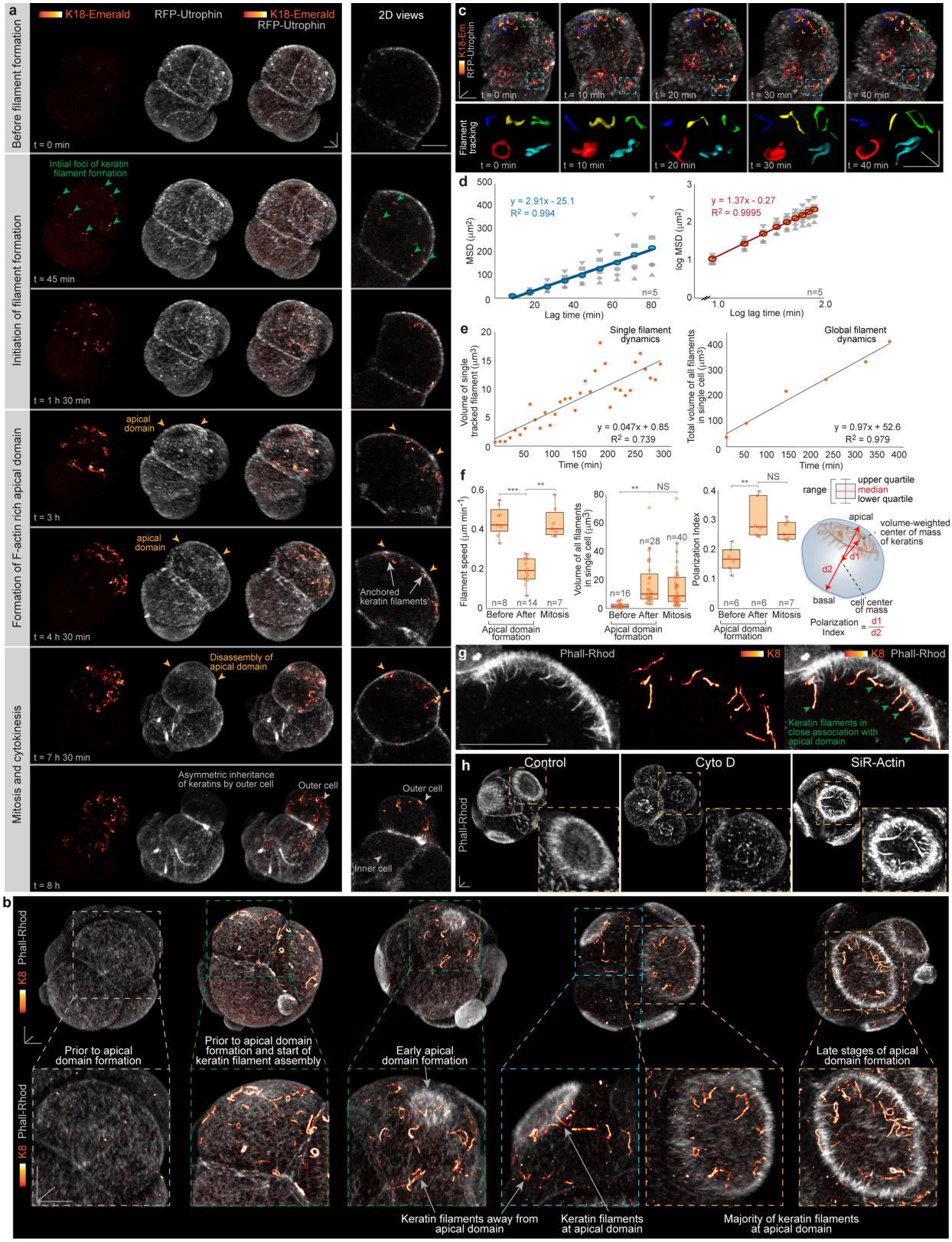

Extended Data Fig. 2 | See next page for caption.

Extended Data Fig. 2 | Tracking and quantitative analysis of keratin filament movement during interphase and mitosis. a, Time series of an embryo expressing K18-Emerald and RFP-Utrophin, with the corresponding major cellular events labelled in the left column. Separate K18-Emerald and RFP-Utrophin channels are shown. Right panels show 2D views through a single cell that assembles keratin filaments, for better visualization of keratin distribution within the cell, relative to the apical domain. Keratin filament assembly is initiated before the formation of the apical domain. When the apical domain forms, keratin filaments become enriched apically in close association with F-actin. During mitosis, the apical domain disassembles but keratin filaments remain apically localized, resulting in their asymmetric inheritance by the outer daughter cell. Data are from three independent experiments. **b**, Immunofluorescence of endogenous keratins in embryos fixed at different stages of apical domain formation recapitulates the pattern and localization of keratin filaments relative to the apical domain observed in live imaging experiments. Data are from three independent experiments. **c**, Computationally-rendered filaments obtained from live imaging data. In this example, five individual filaments were tracked over time with a 10-min interval between frames. Data are from three independent experiments. **d**, The log mean square displacement (MSD) versus log lag time graph indicates that the movement of keratin filaments is unconfined and diffusive (slope > 1). Pearson's correlation. **e**, Volume of an individual keratin filament and total filament volume within a single tracked cell increase linearly over time. Pearson's correlation. **f**, Quantification of filament speed, volume of filaments, and polarization index before apical domain formation, after apical domain formation, and during mitosis. After the formation of the apical domain, keratin filaments move more slowly, display a larger total volume, and become more apically polarized than before apical domain formation. During mitosis, keratin filaments move faster, but retain a large volume and high apical polarization. ***$P = 0.0002$; **$P = 0.001$; Kruskal–Wallis test for filament speed; **$P = 0.003$; ANOVA test for filament volume; **$P = 0.003$; Kruskal–Wallis test for polarization index. Scheme shows the parameters used for calculation of the polarization index. $d1$ is the distance between the volume-weighted centre of mass of the keratin filaments and the centre of mass of the cell. $d2$ is the length of the apical-basal axis of the cell. **g**, High-resolution immunofluorescence images show that keratin filaments align specifically along actin filaments extending from the apical domain. Green arrows indicate examples of keratin–actin colocalization. Data are from three independent experiments. **h**, Differences in F-actin accumulation at the apical domain of control embryos and embryos treated with cytochalasin D or a high concentration of SiR-Actin. Insets show zoomed views of individual 8-cell blastomeres, highlighting the loss of the apical domain in cytochalasin D-treated embryos, and a dense accumulation of apical F-actin in SiR-Actin-treated embryos. Data are from three independent experiments. Scale bars, 10 µm.

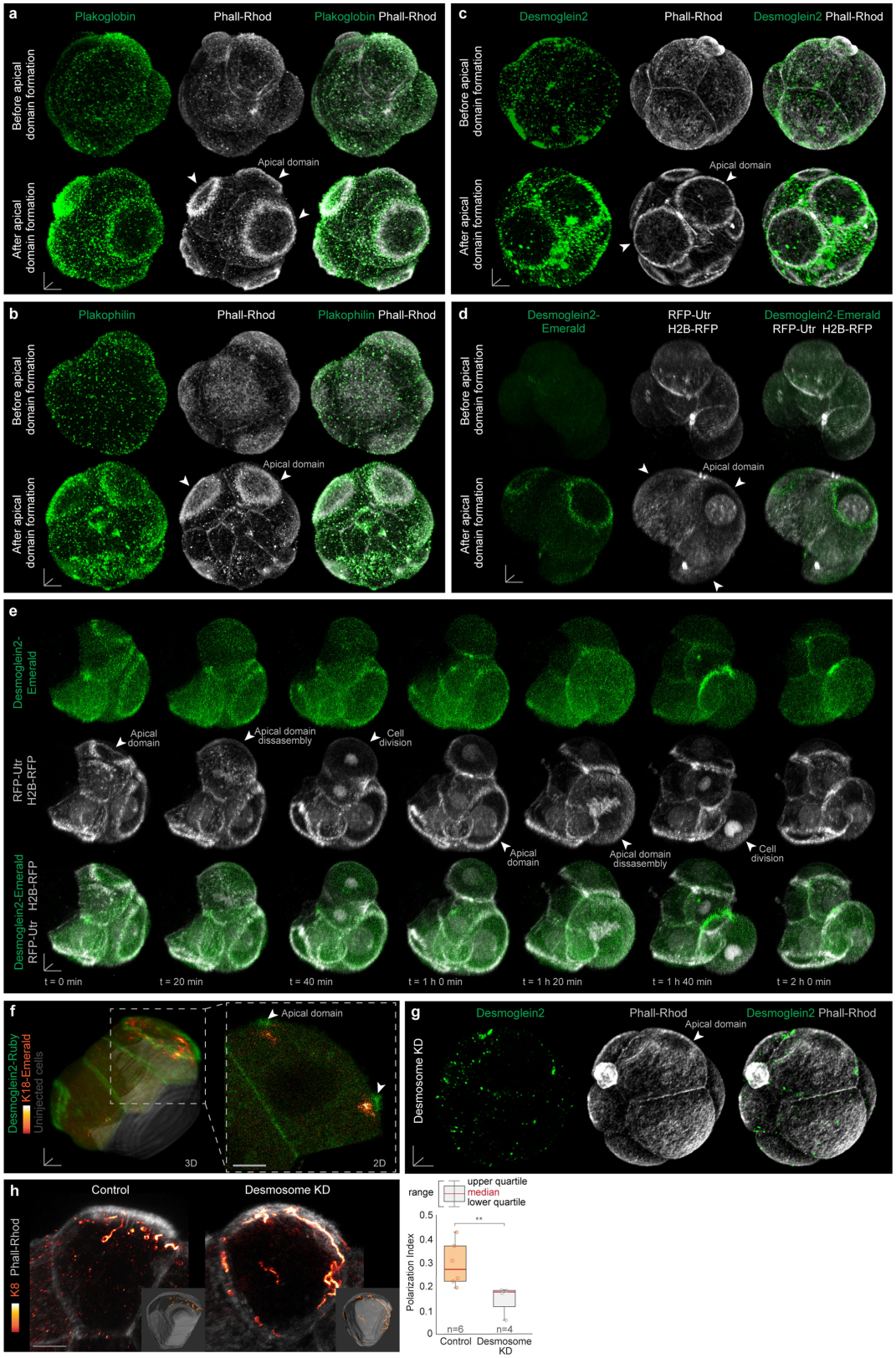

Extended Data Fig. 3 | See next page for caption.

Extended Data Fig. 3 | Apical keratin localization requires desmosome protein components. a–**c**, Immunofluorescence of endogenous plakoglobin (**a**), plakophilin (**b**), and desmoglein2 (**c**) before and after apical domain formation. Apical accumulation of all three desmosome components is observed after apical domain formation. **d**, Live imaging of an embryo expressing desmoglein2-Emerald, RFP-utrophin and H2B-RFP recapitulates the endogenous desmoglein2 expression, both before and after apical domain formation. **e**, Time series of embryo expressing desmoglein2-Emerald, RFP-utrophin and H2B-RFP. Desmoglein2-Emerald accumulates with the apical domain (labelled by RFP-utrophin) during interphase. When the cell enters mitosis, desmoglein2-Emerald disassembles from the apical surface together with the apical domain. White arrows indicate two different mitotic events within the same embryo. **f**, Live embryo expressing desmoglein2-Ruby and K18-Emerald shows the enrichment of keratin filaments at the site of apical desmosome accumulation. **g**, Embryos injected with siRNAs against desmosome components do not accumulate desmoglein2 apically with the apical domain. **h**, Desmosome knockdown causes a more homogenous distribution of keratin filaments, as measured by a polarization index. $^{**}P = 0.01$; unpaired, two-tailed Mann–Whitney *U*-test. Data are from three independent experiments. Scale bars, 10 μm.

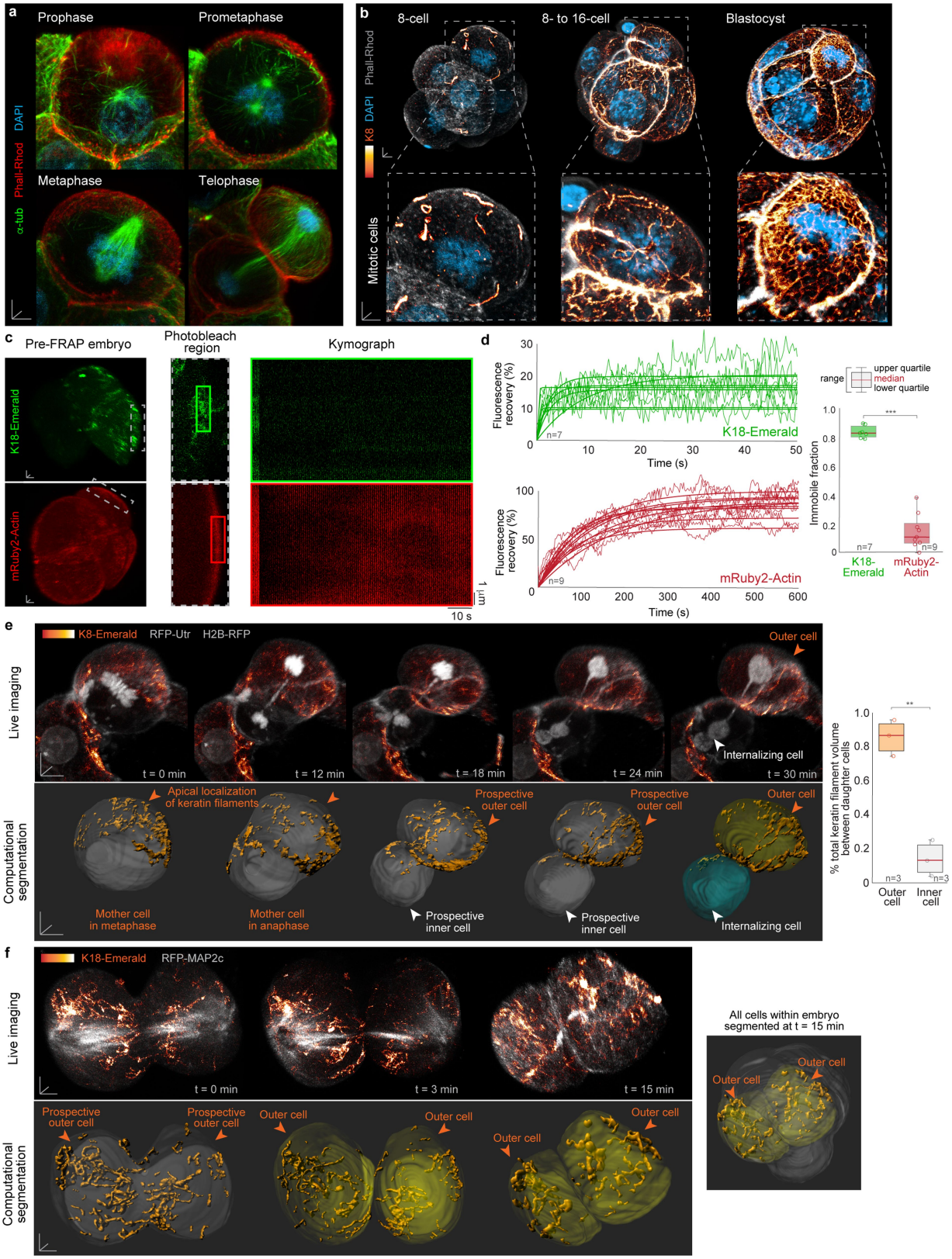

Extended Data Fig. 4 | See next page for caption.

Extended Data Fig. 4 | Keratin filaments are stably retained during mitosis, and become asymmetrically inherited by outer daughter cells. a, Immunofluorescence shows the extensive remodelling of cortical F-actin and microtubules during different stages of mitosis. Data are from six independent experiments. **b**, Immunofluorescence for K8 shows endogenous keratin filaments retained within mitotic cells in embryos fixed at multiple stages of development. Data are from six independent experiments. **c**, FRAP experiments for K18-Emerald and mRuby2-Actin performed in whole live embryos. All cells selected for FRAP were at the eight-cell stage and in interphase, when the actin ring is visible. 3D views of entire pre-FRAP embryos (left), zoomed views of the photobleached regions of interest (middle), and kymographs of pre- and post-FRAP fluorescence intensities (right). Data are from three independent experiments. **d**, Analysis of FRAP experiments. Left graphs show fluorescence recovery of K18-Emerald (green) and mRuby2-Actin (red) over time. Thinner lines represent raw data after normalization, and thicker lines indicate fitted exponential curves. Right graph shows that K18-Emerald has a larger immobile fraction than mRuby2-Actin. $^{***}P < 0.0001$; unpaired, two-tailed Student's *t*-test. **e**, Live imaging of embryos expressing K8-Emerald show a similar pattern of expression and inheritance as K18-Emerald. The outer daughter cell inherits most of the keratin filaments during an outer-inner division (top). Computational segmentation of the same cell at each stage of mitosis (bottom). Quantification of proportion of keratin filaments inherited by outer and inner cells in live embryos expressing K8-Emerald shows a comparable asymmetry in keratin inheritance as K18-Emerald. $^{**}P = 0.001$; unpaired, two-tailed Student's *t*-test. **f**, Time series of a cell expressing K18-Emerald undergoing a symmetric outer-outer division. Keratin filaments are uniformly inherited by both daughter cells during divisions producing two outer cells (top). Computational segmentation of the same cells at each time point (bottom), and whole embryo inset highlighting the outer location of both daughter cells (right). Data are from four independent experiments. Scale bars, 5 μm.

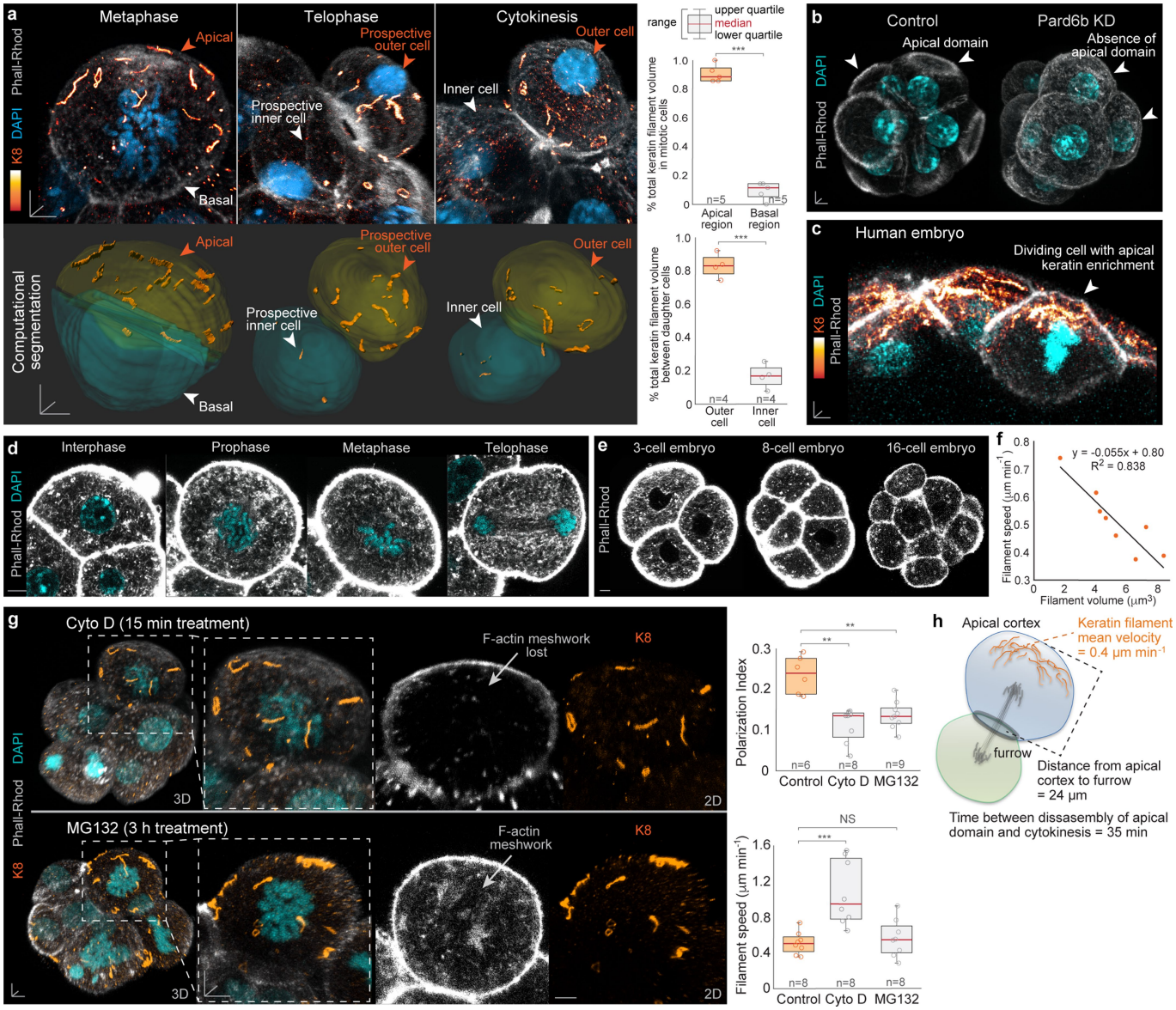

Extended Data Fig. 5 | A dense F-actin meshwork within mitotic cells hinders the movement of keratin filaments away from the apical cortex. **a**, Immunofluorescence of embryos fixed specifically when a cell was undergoing mitosis or cytokinesis. Top, keratin filaments remain apically-localized throughout different mitotic stages, and become inherited by the prospective outer cell. Bottom, computational segmentation of the same cells highlighting the apical keratin distribution and asymmetric keratin inheritance. Quantification of proportion of endogenous keratin filaments present in the apical and basal regions of mitotic cells, and between prospective outer and inner daughter cells, showing a comparable asymmetry in endogenous keratin localization and inheritance as K18-Emerald dynamics in live embryos. ***$P < 0.0001$; unpaired, two-tailed Student's t-test. **b**, Embryos microinjected with *Pard6b* siRNAs do not form an apical F-actin ring in the eight-cell embryo. Data are from three independent experiments. **c**, Mitotic cell within a fixed human embryo also displays an apical localization of keratins. **d**, A dense cytoplasmic F-actin meshwork is maintained throughout interphase and all stages of mitosis. Data are from three independent experiments. **e**, The F-actin meshwork is also present in cells across different stages of development. Representative images of a 3-cell, compacted 8-cell, and 16-cell embryo with all cells displaying a dense cytoplasmic F-actin meshwork. Data are from three independent experiments. **f**, Analysis of keratin filament movement during mitosis reveals that filament speed is inversely related to filament volume. $n = 8$ filaments; Pearson's correlation. **g**, Acute cytochalasin D treatment for 15 min specifically during mitosis disrupts the F-actin meshwork, reduces the apical localization of keratins, and increases keratin filament speed. Cells treated with MG132 for 3 h retain an F-actin meshwork, but keratin apical localization is reduced and filament speed is unchanged. **$P = 0.002$ for CytoD; **$P = 0.01$ for MG132; Kruskal–Wallis test for polarization index; ***$P = 0.0005$; ANOVA test for filament speed. **h**, Scheme of a cell division producing an inner (green) and an outer (blue) cell. Keratin filaments localize close to the apical cortex of the forming outer daughter cell. The distance between the apical cortex and cytokinetic furrow, time between disassembly of the apical F-actin domain and cytokinesis, and the mean speed of keratin filament movement are indicated. Scale bars, 5 μm.

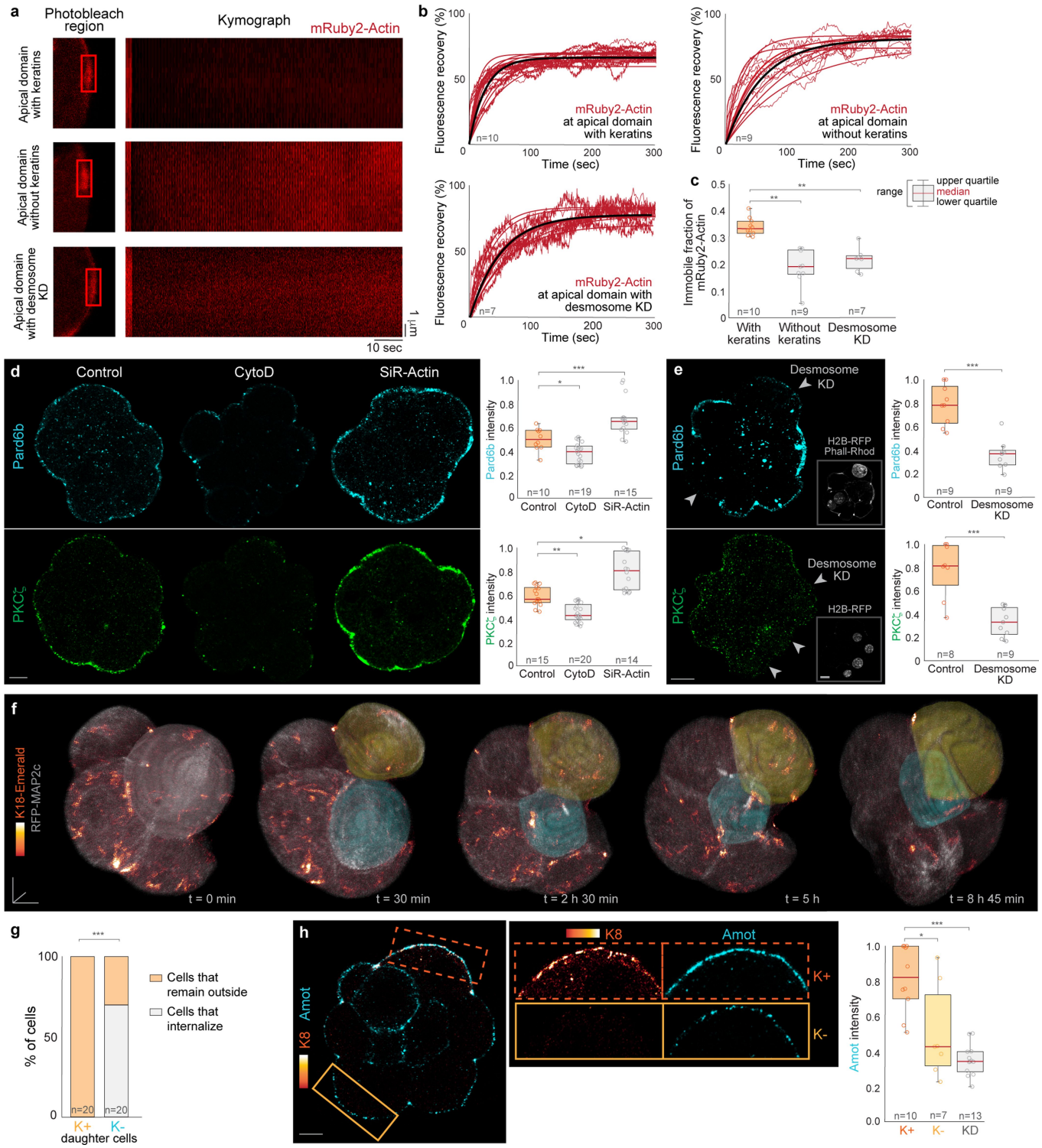

Extended Data Fig. 6 | See next page for caption.

Extended Data Fig. 6 | Keratins promote actin stability and apical polarization. a, FRAP experiments for mRuby2-Actin performed at the apical domain of interphase cells with keratins, cells without keratins, and cells microinjected with desmosome siRNAs. Selected photobleached regions of interest (left) and kymographs of pre- and post-FRAP fluorescence intensities (right) are shown. Data are from three independent experiments. **b**, Analysis of FRAP experiments. Graphs show the fluorescence recovery of mRuby2-Actin over time for each condition. Thinner red lines indicate raw data after normalization, thicker red lines are fitted exponential curves, and thick black lines represent the mean fitted exponential curves. **c**, Cells lacking keratins and cells with reduced desmosome expression show a smaller immobile fraction of mRuby2-Actin compared to cells with keratins. $^{**}P = 0.0002$ for without keratins; $^{**}P = 0.003$ for desmosome KD; Kruskal–Wallis test. **d**, Immunofluorescence of 16-cell stage control embryos and embryos treated with cytochalasin D and SiR-Actin. Disruption of actin stability using cytochalasin D reduces accumulation of apical polarity markers PARD6B and PKCζ. By contrast, increasing actin stability using SiR-Actin increases apical polarity levels. $^{*}P = 0.03$; $^{***}P = 0.0009$; ANOVA test for PARD6B; $^{*}P = 0.03$; $^{**}P = 0.003$; Kruskal–Wallis test for PKCζ. **e**, Desmosome knockdown in 16-cell stage embryos reduces levels of apical polarity markers PARD6B and PKCζ. $^{***}P = 0.0002$ for PARD6B; $^{***}P = 0.001$ for PKCζ; Unpaired, two-tailed Mann–Whitney *U*-test. **f**, Live imaging of K18-Emerald in an embryo displaying a cell division. After division, the daughter cell that did not inherit keratins (cyan) undergoes apical constriction to form the pluripotent inner cell mass[35], whereas the outer daughter cell that inherited keratins (yellow) does not internalize. Data are from three independent experiments. **g**, Analysis of internalization events in cells that inherited (K+) or did not inherit (K–) keratin filaments after division. $^{***}P < 0.0001$; two-tailed Fisher's exact test. **h**, Immunofluorescence of endogenous K8 and AMOT in a 16-cell stage embryo. Right panels indicate zoomed views of the apical region of cells with and without keratins, with separate K8 and AMOT channels for better visualization. Cells with keratins display higher levels of apical AMOT than cells lacking keratins and cells with K8 and K18 knockdown. $^{*}P = 0.04$; $^{***}P < 0.0001$; Kruskal–Wallis test. Scale bars, 10 µm.

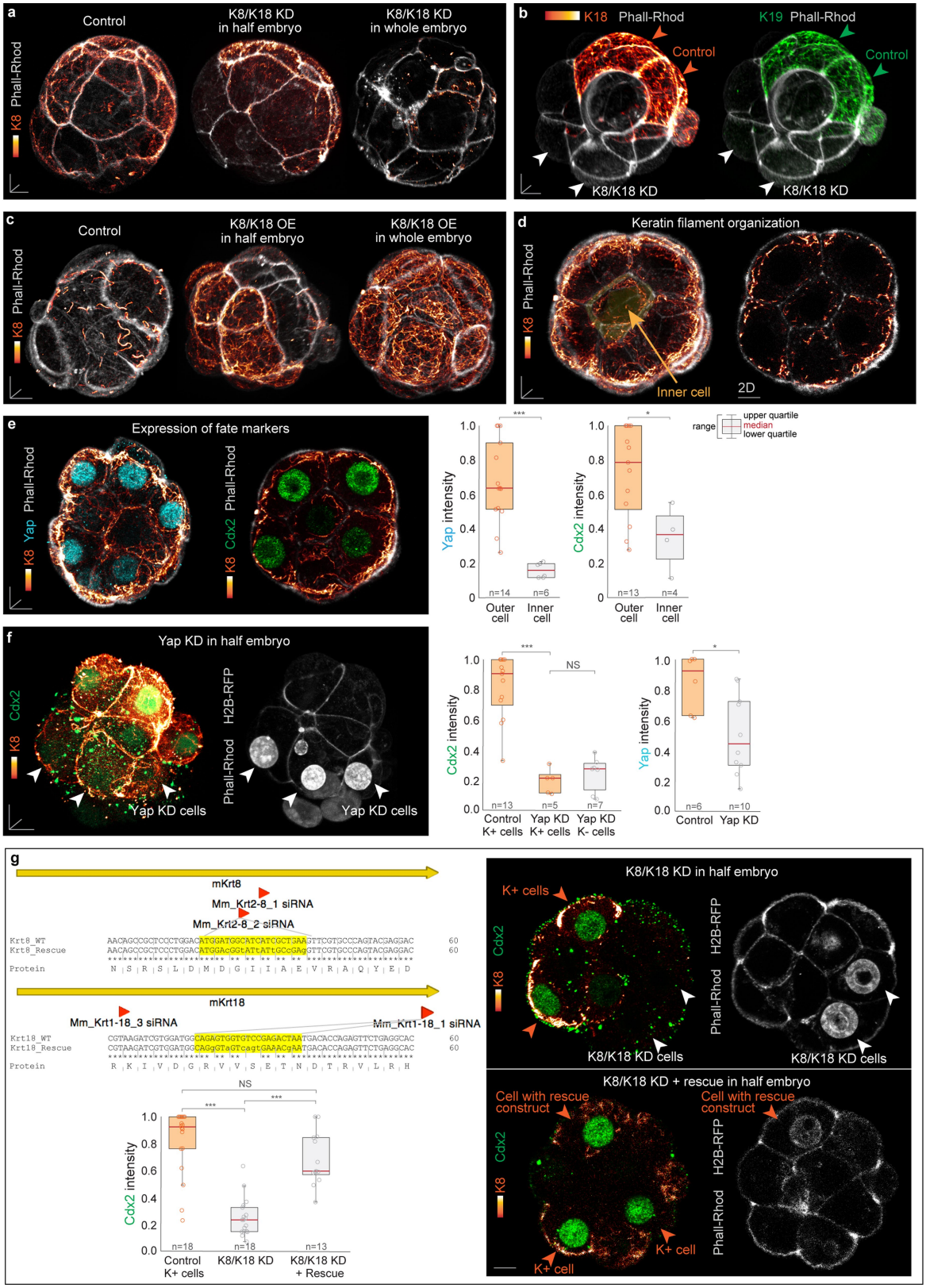

Extended Data Fig. 7 | See next page for caption.

Extended Data Fig. 7 | Experimental manipulations of keratin levels show that keratins regulate CDX2 to specify the first trophectoderm cells of the embryo. a, Immunofluorescence for K8 in embryos microinjected with siRNAs for K8 and K18 at the one-cell stage, or into only one cell at the two-cell stage. This double-knockdown approach extensively eliminates keratin filament assembly. Data are from five independent experiments. **b**, Knockdown of K8 and K18 in half of the embryo also eliminates filament formation by K19. White arrowheads show knockdown cells. Data are from three independent experiments. **c**, Keratin overexpression causes a premature and widespread assembly of a keratin network within the 8- to 16-cell stage embryo. Images show examples of embryos microinjected with high levels of *K8* and *K18* RNA at the 1-cell stage, or into one cell of the 2-cell embryo. Data are from three independent experiments. **d**, Keratin overexpression causes some filaments to be inherited by inner cells of the 16-cell stage embryo (yellow segmented cell indicated by arrow in left panel). 2D view shows keratin filament organization within outer and inner cells of keratin overexpressing embryos (right). Data are from three independent experiments. **e**, Inner cells in keratin overexpressing embryos express lower levels of nuclear YAP and CDX2 than outer cells. $^{*}P = 0.04$; $^{***}P < 0.0001$; unpaired, two-tailed Mann–Whitney *U*-test. **f**, Knockdown of YAP using siRNAs microinjected into one cell of the two-cell embryo reduces CDX2 levels, in both keratin-positive and keratin-negative cells. H2B-RFP was co-injected with the siRNAs to identify the knockdown cells (white arrowheads). $^{***}P < 0.0001$; ANOVA test for CDX2. Right graph shows that our knockdown approach using *YAP* siRNAs effectively reduced YAP levels. $^{*}P = 0.03$, unpaired, two-tailed Mann–Whitney *U*-test for YAP. **g**, Scheme depicting cloning strategy to generate rescue constructs for K8 and K18. The coding regions of K8 and K18 are indicated by thick yellow arrows, and the targeted sequence locations for the keratin siRNAs used in this study are indicated by the red arrows. The specific siRNA target sequences are highlighted in yellow, corresponding to the keratin wild-type (WT) sequence (top rows). The rescue construct sequences are indicated (bottom rows). Note the conservation of amino acid sequence despite the scrambling of DNA bases throughout the siRNA target sequence. In each experiment, H2B-RFP was co-injected with the siRNAs and/or mRNAs to label the injected half of the embryo, and 100% of H2B-positive cells displayed keratin filaments when injected with the rescue construct. K8/K18-knockdown cells express lower levels of CDX2 than control cells with keratins, but this phenotype is rescued when the keratin rescue constructs are co-injected with keratin siRNAs. $^{***}P < 0.0001$; ANOVA test. Scale bars, 10 µm.

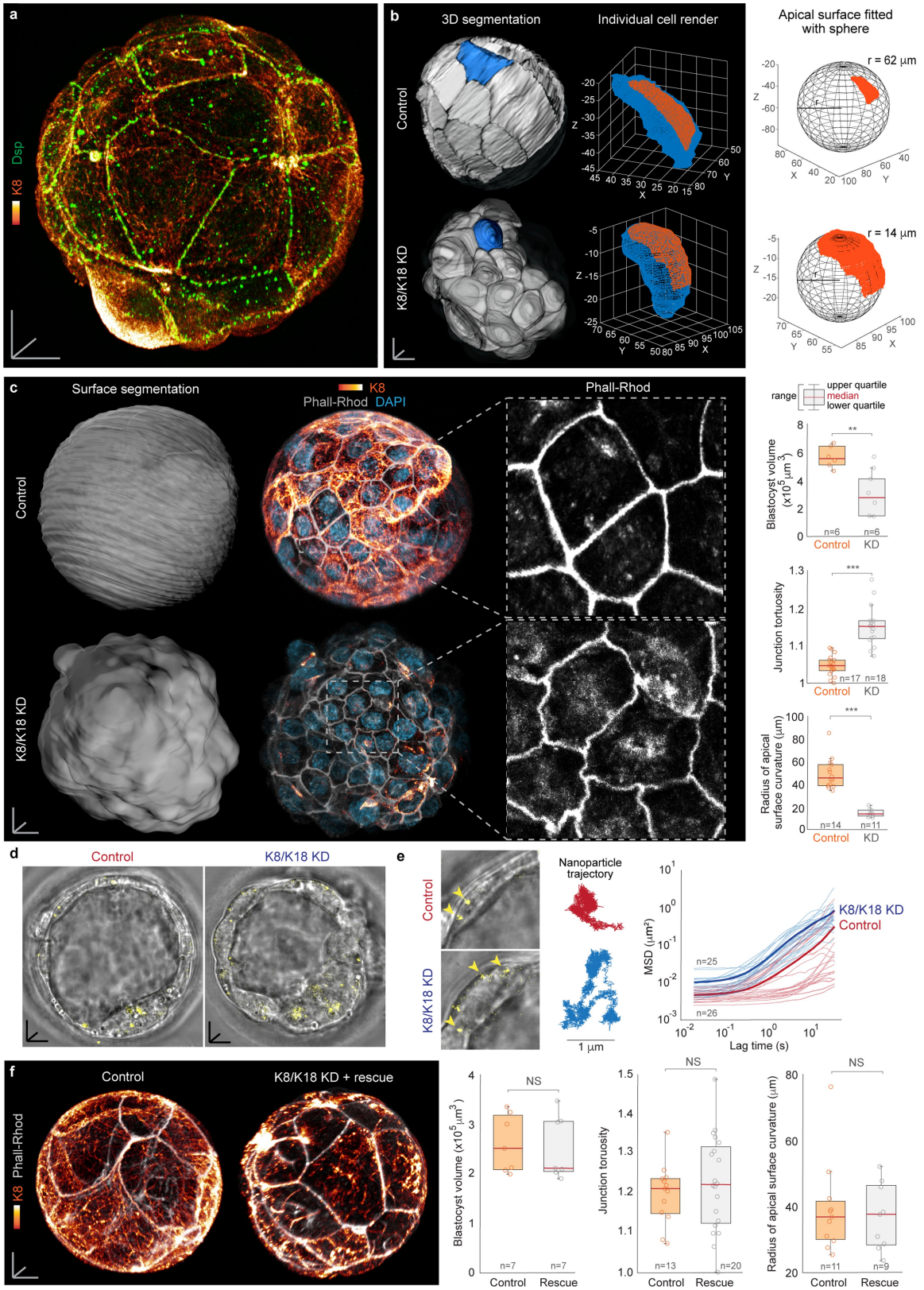

Extended Data Fig. 8 | See next page for caption.

Extended Data Fig. 8 | Keratins regulate blastocyst morphogenesis. **a**, Punctate desmosome structures labelled using immunofluorescence for desmoplakin (Dsp) colocalize with K8 along the trophectoderm cell–cell junctions of the blastocyst. Data are from three independent experiments. **b**, Analysis of apical surface curvature in control and K8/K18-knockdown blastocysts. Individual cells within the intact embryo were computationally-segmented in 3D. Single cells (blue) are selected for apical surface analysis. Middle panels show rendering of the apical surfaces (orange) of the selected cells. The right panels show fitting of the cell apical surface to a sphere for calculation of radius of apical surface curvature. Data are from three independent experiments. **c**, K8/K18-knockdown blastocysts display morphogenetic defects, revealed by smaller blastocyst volume, higher junctional tortuosity, and trophectoderm cells with lower radius of apical surface curvature. $^{**}P = 0.004$ for blastocyst volume; $^{***}P < 0.0001$ for junctional tortuosity; $^{***}P < 0.0001$ for surface curvature; unpaired, two-tailed Mann–Whitney *U*-test. **d**, 2D confocal planes of live control and K8/K18-knockdown blastocysts, microinjected with fluorescent nanoparticles (yellow). Data are from three independent experiments. **e**, Images show nanoparticles within single trophectoderm cells, in control and K8/K18-knockdown embryos. Middle panels show representative trajectories of nanoparticle movement. Graph shows their mean squared displacement (MSD) over lag time. Thicker lines represent the mean of individual curves. The graph has two phases revealing different cytoskeletal properties: a time-independent (short lag times) and a time-dependent (long lag times) phase. These phases are associated with elasticity and viscosity, respectively[40]. Differences in MSD during the time-independent phase reveal higher elasticity, indicative of lower cytoplasmic stiffness, in the K8/K18-knockdown cells. **f**, Co-injection of keratin rescue constructs with K8/K18 siRNAs can restore blastocyst morphology to control conditions. Unpaired, two-tailed Student's *t*-test for blastocyst volume and surface curvature; unpaired, two-tailed Mann–Whitney *U*-test for junction tortuosity; NS, not significant. Scale bars, 10 µm.

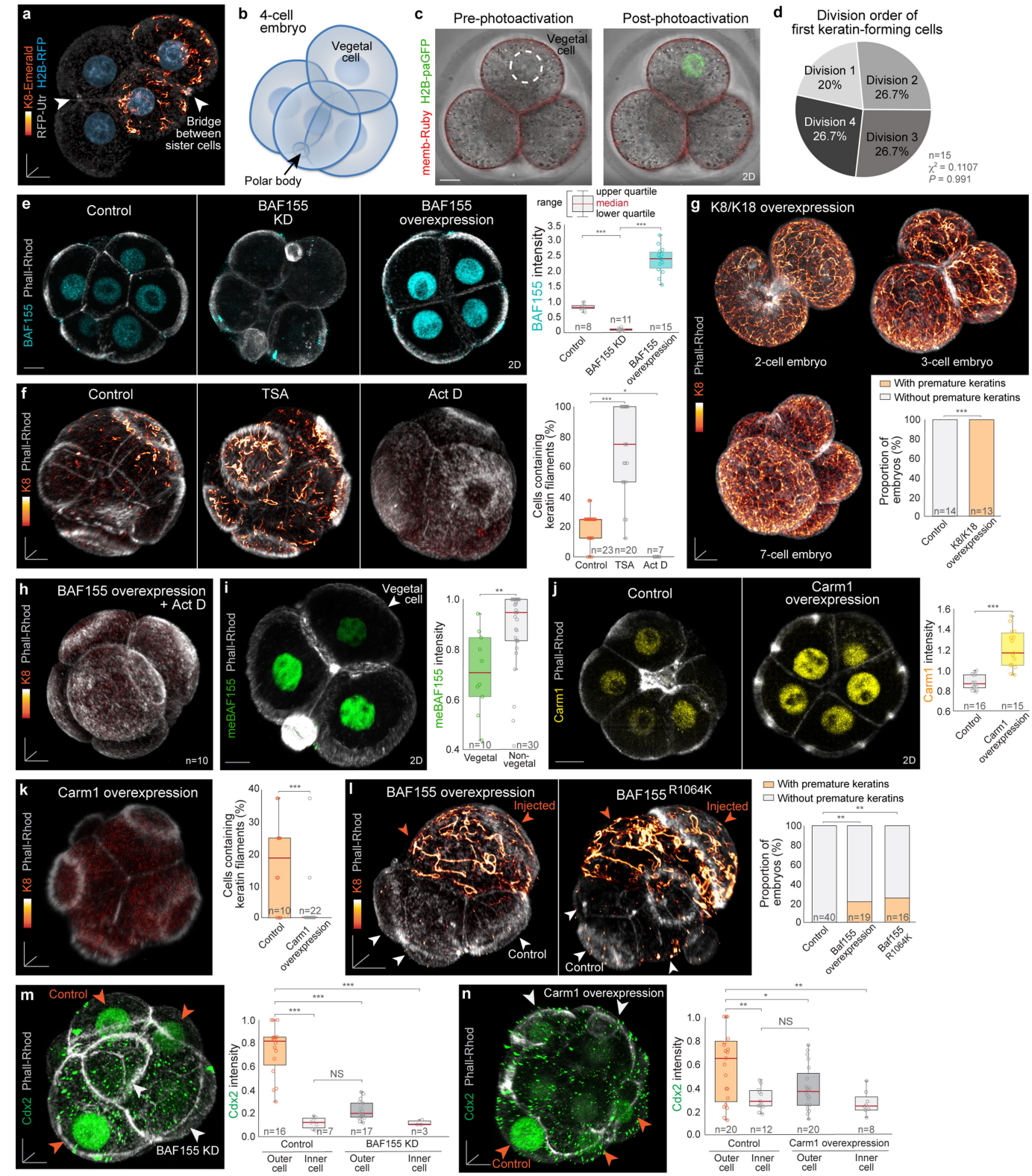

Extended Data Fig. 9 | See next page for caption.

Extended Data Fig. 9 | Heterogeneities in BAF155 and CARM1 within the early embryo trigger differential expression of keratins at the eight-cell stage. a, Live-imaging of an embryo expressing K8-Emerald, H2B-RFP and RFP-Utrophin confirms that the first cells to assemble keratin filaments are sister cells. The microtubule bridge connecting sister cells can be identified by RFP-Utrophin accumulation (white arrowheads)[41]. Data are from three independent experiments. **b**, Scheme shows the stereotypical 3D organization of a tetrahedral four-cell embryo. The vegetal blastomere is located distal from the polar body. **c**, Selective photoactivation of the vegetal blastomere. The vegetal blastomere is identified based on its distal position from the polar body. The vegetal cell nucleus is then targeted with a two-photon laser (820 nm light) to photoactivate H2B-paGFP. 2D confocal planes show efficient photoactivation immediately after 820 nm light illumination. Data are from three independent experiments. **d**, The first cells to form keratin filaments are unrelated to the order of cell divisions during the 4- to 8-cell stage transition. χ^2 test. **e**, BAF155 knockdown reduces BAF155 immunofluorescence levels relative to control blastomeres, while BAF155 overexpression increases them. Embryos were microinjected with *BAF155* siRNAs or high levels of *BAF155* RNA respectively at the one-cell stage. ***$P < 0.0001$; ANOVA test. **f**, Embryos treated with trichostatin A (TSA) display extensive keratin filament formation, while embryos treated with actinomycin D (Act D) do not form filaments. *$P = 0.0489$; ***$P < 0.0001$; ANOVA test. **g**, Microinjection of *K8* and *K18* mRNA into the one-cell embryo causes premature assembly of an extensive keratin filament network throughout early blastomeres before the eight-cell stage. ***$P < 0.0001$; two-sided Fisher's exact test. **h**, BAF155-overexpressing embryos treated with actinomycin D do not form keratin filaments at the eight-cell stage. Data are from three independent experiments. **i**, Dimethyl-BAF155 is lowest in the vegetal blastomere. **$P = 0.004$; unpaired, two-tailed Student's *t*-test. **j**, CARM1 overexpression increases CARM1 immunofluorescence levels relative to control blastomeres. Embryos were microinjected with high levels of *Carm1* RNA at the 1-cell stage. ***$P < 0.0001$; unpaired, two-tailed Mann–Whitney *U*-test. **k**, CARM1 overexpression reduces keratin filament assembly. ***$P = 0.0007$; unpaired, two-tailed Student's *t*-test. **l**, Overexpression of BAF155 or mutant BAF155(R1064K) causes premature keratin filament assembly at the four-cell stage. **$P = 0.009$ for BAF155 overexpression; **$P = 0.005$ for BAF155(R1064K); two-sided Fisher's exact test. **m**, BAF155-knockdown blastomeres (white arrowheads) display lower levels of CDX2 than control cells (orange arrowheads) at the same stage. *BAF155* siRNAs were microinjected into only one cell of the two-cell embryo. ***$P < 0.0001$; ANOVA test. **n**, CARM1-overexpression blastomeres (white arrowheads) display lower levels of CDX2 than control blastomeres (orange arrowheads) at the same stage. High levels of *Carm1* RNA were microinjected into only one cell at the two-cell stage. **$P = 0.005$ for control inner cells; *$P = 0.04$ for CARM1 overexpression outer cells; **$P = 0.006$ for CARM1-overexpression inner cells; ANOVA test. Scale bars, 10 µm.

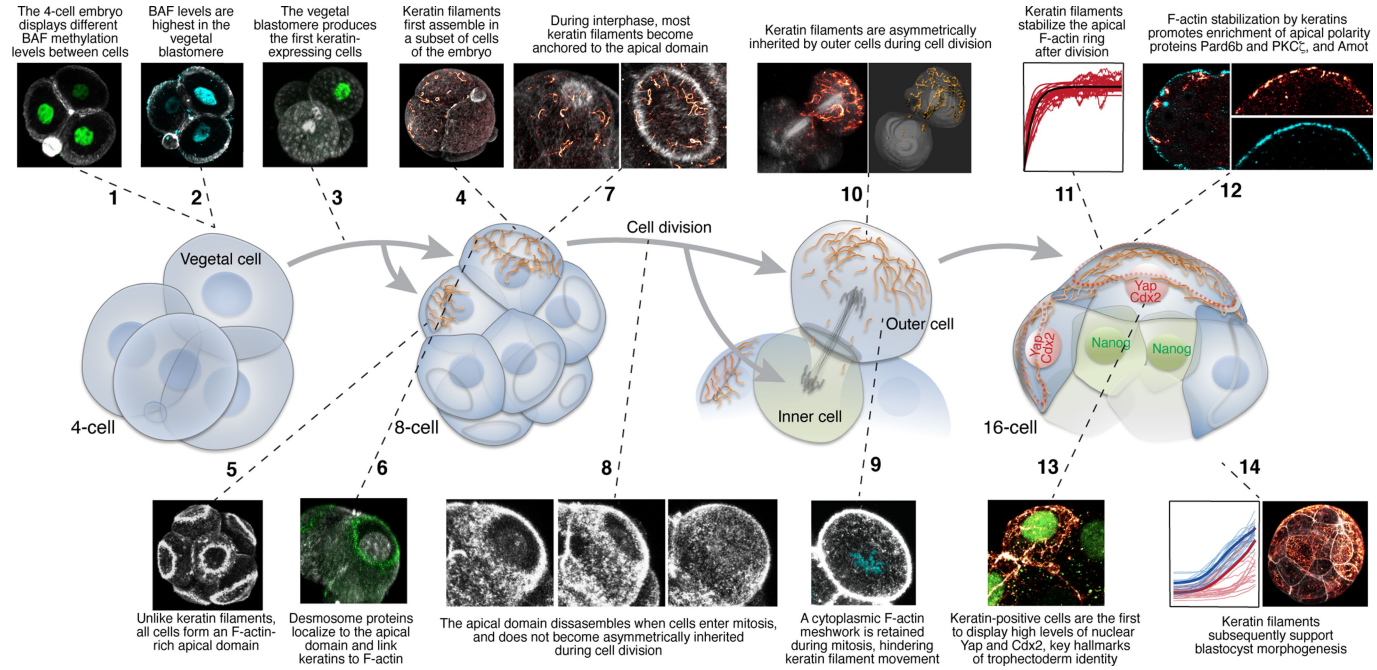

Extended Data Fig. 10 | Scheme summarizing the main findings. Keratin expression is regulated by early heterogeneities in the BAF complex. During inner–outer cell segregation, apically localized keratin filaments are asymmetrically inherited by outer daughter cells, where they stabilize apical F-actin to promote apical polarity and acquisition of a trophectoderm fate. At late stages, keratins also support blastocyst morphogenesis. The numbers indicate the key events.

nature research

Corresponding author(s): Nicolas Plachta

Last updated by author(s): Jun 2, 2020

Reporting Summary

Nature Research wishes to improve the reproducibility of the work that we publish. This form provides structure for consistency and transparency in reporting. For further information on Nature Research policies, see Authors & Referees and the Editorial Policy Checklist.

Statistics

For all statistical analyses, confirm that the following items are present in the figure legend, table legend, main text, or Methods section.

n/a	Confirmed	
☐	☒	The exact sample size (*n*) for each experimental group/condition, given as a discrete number and unit of measurement
☐	☒	A statement on whether measurements were taken from distinct samples or whether the same sample was measured repeatedly
☐	☒	The statistical test(s) used AND whether they are one- or two-sided *Only common tests should be described solely by name; describe more complex techniques in the Methods section.*
☒	☐	A description of all covariates tested
☐	☒	A description of any assumptions or corrections, such as tests of normality and adjustment for multiple comparisons
☐	☒	A full description of the statistical parameters including central tendency (e.g. means) or other basic estimates (e.g. regression coefficient) AND variation (e.g. standard deviation) or associated estimates of uncertainty (e.g. confidence intervals)
☐	☒	For null hypothesis testing, the test statistic (e.g. *F*, *t*, *r*) with confidence intervals, effect sizes, degrees of freedom and *P* value noted *Give P values as exact values whenever suitable.*
☒	☐	For Bayesian analysis, information on the choice of priors and Markov chain Monte Carlo settings
☒	☐	For hierarchical and complex designs, identification of the appropriate level for tests and full reporting of outcomes
☒	☐	Estimates of effect sizes (e.g. Cohen's *d*, Pearson's *r*), indicating how they were calculated

Our web collection on statistics for biologists contains articles on many of the points above.

Software and code

Policy information about availability of computer code

Data collection	Time-lapse imaging of live samples and single confocal scans of fixed immunostained samples were both performed using Zeiss ZEN software, on a Zeiss LSM 780 or LSM 880.
Data analysis	All image analyses were performed using Imaris 8.2 (Bitplane AG), Fiji, and MATLAB (Version R2018a). Statistical analyses were performed using GraphPad Prism (Version 8.3) and Microsoft Excel (Version 16.3). Custom code has been deposited in a publicly available repository at https://github.com/gracelhy/Analysis-of-embryo-parameters

For manuscripts utilizing custom algorithms or software that are central to the research but not yet described in published literature, software must be made available to editors/reviewers. We strongly encourage code deposition in a community repository (e.g. GitHub). See the Nature Research guidelines for submitting code & software for further information.

Data

Policy information about availability of data

All manuscripts must include a data availability statement. This statement should provide the following information, where applicable:

- Accession codes, unique identifiers, or web links for publicly available datasets
- A list of figures that have associated raw data
- A description of any restrictions on data availability

Source Data behind Figs. 1 to 4 and Extended Data Figs. 3 to 10 are available within the manuscript files.

Field-specific reporting

Please select the one below that is the best fit for your research. If you are not sure, read the appropriate sections before making your selection.

☒ Life sciences ☐ Behavioural & social sciences ☐ Ecological, evolutionary & environmental sciences

For a reference copy of the document with all sections, see nature.com/documents/nr-reporting-summary-flat.pdf

Life sciences study design

All studies must disclose on these points even when the disclosure is negative.

Sample size	No statistical test was performed to determine sample size. Sample size was determined based on prior experience and typical ranges used by research groups in the preimplantation mouse embryo field, and also in accordance to statistical test requirements. Previous work utilizing similar sample sizes includes Zenker et al. 2018 Cell 173:776-791; Zenker et al. 2017 Science 357: 925-928; White et al. 2016 Cell 165(1): 75-87.
Data exclusions	Embryos excluded from analyses include: 1) Unsuccessfully microinjected embryos that display low or undetectable fluorescence labeling unsuitable for quantitative analysis, and 2) 10-15% of embryos that display arrested or slower development in culture conditions. These exclusion criteria have been utilized in our previous work.
Replication	All experiments in this study were successfully performed at least 3 times with different batches of embryos, mRNA or siRNA preparations.
Randomization	Embryos were randomly allocated into experimental groups. All embryos and cells within embryos were randomly selected for analysis.
Blinding	Successfully developed and imaged embryos have to be selected for subsequent analysis. Therefore, investigators were only blinded for computational analysis following acquisition of imaging data.

Reporting for specific materials, systems and methods

We require information from authors about some types of materials, experimental systems and methods used in many studies. Here, indicate whether each material, system or method listed is relevant to your study. If you are not sure if a list item applies to your research, read the appropriate section before selecting a response.

Materials & experimental systems

n/a	Involved in the study
☐	☒ Antibodies
☒	☐ Eukaryotic cell lines
☒	☐ Palaeontology
☐	☒ Animals and other organisms
☐	☒ Human research participants
☒	☐ Clinical data

Methods

n/a	Involved in the study
☒	☐ ChIP-seq
☒	☐ Flow cytometry
☒	☐ MRI-based neuroimaging

Antibodies

Antibodies used

Primary antibodies:
Rat monoclonal anti-Keratin 8 (DSHB, TROMA-I) used at 1:20.
Rabbit polyclonal anti-Keratin 18 (Sigma, SAB4501665, Lot #310243) used at 1:200.
Rat monoclonal anti-Keratin 19 (DSHB, TROMA-III) used at 1:50.
Mouse monoclonal anti-Pan-keratin (Cell Signaling, 4545) used at 1:50.
Mouse monoclonal anti-alpha-tubulin (Sigma, T6199) used at 1:1000.
Mouse monoclonal anti-Pard6b (Santa Cruz, 166405) used at 1:50.
Mouse monoclonal anti-PKCzeta (Santa Cruz, 17781) used at 1:50.
Rabbit monoclonal anti-Yap (Cell Signaling, 8418S) used at 1:500.
Rabbit polyclonal anti-Cdx2 (Abcam, 88129) used at 1:200.
Rabbit polyclonal anti-Nanog (Abcam, 80892) used at 1:200.
Guinea pig polyclonal anti-Desmoplakin1 (Progen, DP-1) used at 1:100.
Mouse monoclonal anti-Desmoglein1/2 (Progen, 61002S) used undiluted.
Mouse monoclonal anti-Plakophilin2 (Progen, 651101S) used undiluted.
Mouse monoclonal anti-Plakoglobin (Progen, 61005S), used undiluted.
Mouse monoclonal anti-BAF155 (Santa Cruz, 48350) used at 1:50.
Rabbit monoclonal anti-Carm1 (Cell Signaling, 3379S) used at 1:150.
Rabbit polyclonal anti-dimethyl-BAF155 Arg1064 (Merck, ABE1339, Lot #3174767) used at 1:100.

Secondary antibodies:

Alexa Fluor 488 Goat anti-Mouse (Invitrogen) used at 1:500.
Alexa Fluor 488 Goat anti-Rat (Invitrogen) used at 1:500.
Alexa Fluor 488 Goat anti-Rabbit (Invitrogen) used at 1:500.
Alexa Fluor 647 Goat anti-Mouse (Invitrogen) used at 1:500.
Alexa Fluor 647 Goat anti-Rat (Invitrogen) used at 1:500.
Alexa Fluor 647 Goat anti-Rabbit (Invitrogen) used at 1:500.
Alexa Fluor 488 Donkey anti-Guinea pig (Jackson ImmunoResearch, 706-545-148) used at 1:500.

Validation

All antibodies were previously validated by vendors and/or published work. Relevant studies include:
Keratin 8: filamentous keratin network in ES cells (Schwarz et al. 2015 Sci. Rep. 5: 9007); keratin network in mouse blastocysts showing trophectoderm-specific localization (Ralston and Rossant 2008 Dev. Biol. 313: 614-629).
Keratin 18: Validation by manufacturer shows specific filamentous staining of HeLa cells in the presence of the antibody; specific staining in notochordal cells (Rodrigues-Pinto et al. 2016 J Orthop Res 34(8):1327-1340).
Keratin 19: Expression in mouse embryonic mammary glands, as expected and colocalizing with other keratin subtypes within the same tissue (Sun et al. 2010 Histochem Cell Biol 133:213-221).
Pan-keratin: Expression in cervical carcinoma tissues, with keratins as known biomarkers (He et al. 2019 Cell Rep 26(10):2636-2650); Specific staining at the interface of a tumor-stromal in vitro assay (Begum et al. 2019 Sci Rep 9:11187).
Alpha-tubulin: Specific localization to interphase and cytokinetic microtubule bridges in mouse embryos (Zenker et al. 2017 Science 357: 925-928); specific localization to mitotic spindles in mouse embryos (Zenker et al. 2018 Cell 173: 776-791).
Pard6b: Specific apical localization in polarized cells, and disruption of cell organization results in its mislocalization (Choi et al. 2019 J Cell Biol 218(7): 2277-2293).
PKCzeta: Staining shows specific apical localization in compacted 8-cell blastomeres of the mouse embryo (Zhu et al. 2017 Nat. Comms. 8:1-16); specific enrichment at apical membranes of outer cells of the mouse embryo, which is disrupted by Pard6b shRNA (Alarcon 2010 Biol. Reprod. 83:347-358).
Yap: Specific staining of nuclei of polar outer cells of the mouse embryo (Anani et al. 2014 Development 141:2813–2824).
Cdx2: Specific staining of nuclei in mouse embryos throughout preimplantation development, and elevated levels in trophectoderm cells of the blastocyst relative to those of the inner cell mass (White et al. 2016 Cell 165:75-87); specific staining of nuclei in morula-stage embryos (Samarage et al. 2015 Dev. Cell 34:435-447).
Nanog: Specific staining of nuclei in mouse embryos (White et al. 2016 Cell 165:75-87); specific staining of inner cell mass nuclei in mouse blastocysts (Panamarova et al. 2016 Development 143:1271-1283).
Desmoplakin1: Punctate staining along cell-cell junctions of trophectoderm cells in the blastocyst, as expected for desmosomal complexes in epithelia (Schwarz et al. 2015 Sci. Rep. 5:9007).
Desmoglein1/2: Specific punctate staining along cell-cell junctions of keratinocytes, as expected (Price et al. 2018 Nat Comms 9:5284).
Plakophilin2: Specific localization along cell-cell junctions of cardiomyocytes (Merkel et al. 2019 Mol Biol Cell 30(21):2639-2650).
Plakoglobin: Membrane localization along cell-cell junctions of keratinocytes, as expected (Dayal et al. 2014 J Cell Sci 127:740-751).
BAF155: Validation by manufacturer shows specific nuclei staining in fixed HeLa cells.
Carm1: Specific staining of nuclei in mouse embryos (White et al. 2016 Cell 165:75-87).
Dimethyl-BAF155: Staining of normal and tumor breast tissue sections (Wang et al. 2014 Cancer Cell 25:21-36).

Animals and other organisms

Policy information about studies involving animals; ARRIVE guidelines recommended for reporting animal research

Laboratory animals	C57BL/6 wild-type female mice were superovulated using 5 iu of pregnant mare serum (PMS, National Hormone and Peptide Program) gonadotropin given intraperitoneally and 5 iu of recombinant chorionic gonadotrophin (CG, National Hormone and Peptide Program) given 48 h after and immediately before mating, according to animal ethics guidelines of the Agency for Science, Technology and Research, Singapore.
Wild animals	No wild animals were used.
Field-collected samples	No field-collected samples were used.
Ethics oversight	Mouse embryo work was performed according to animal ethics guidelines of the Agency for Science, Technology and Research, Singapore. All protocols (IACUC #181370) were approved by the Biological Resource Centre IACUC Committee.

Note that full information on the approval of the study protocol must also be provided in the manuscript.

Human research participants

Policy information about studies involving human research participants

Population characteristics	Embryo donors were carefully selected to meet strict research inclusion criteria to minimize potential risks to the donors. Female donors were between the ages of 20 to 40 years old and had at least one healthy baby at the Center for Reproductive Medicine, Sixth Affiliated Hospital of Sun Yat-Sen University.
Recruitment	Participation in this study was entirely voluntary and no financial inducements were given for embryo donation. Embryo donors were informed that their donated surplus embryos would be used to study the developmental mechanisms of human embryos and that their donation would not affect their IVF cycle. All embryo donors signed informed consent forms stating clearly the goals of the research, potential benefits and risks, and steps taken to ensure that their privacy was met. Conditions of donation: not for profit. Given that only surplus embryos that were not used for IVF could be donated to this study, there could be a bias in

terms of the quality or condition of embryos used for research, and it is unclear whether these surplus embryos could develop to term if implanted in the uterus.

Ethics oversight

This work was approved by the Ethics Committee of Center for Reproductive Medicine, Sixth Affiliated Hospital of Sun Yat-Sen University (Research license 2019SZZX-008). The Medicine Ethics Committee of Center for Reproductive Medicine, Sixth Affiliated Hospital of Sun Yat-Sen University is composed of 11 members, including experts of laws, scientists and clinicians with relevant expertise. The Committee evaluated the scientific merit and ethical justification of this study and conducted a full review of the donations and use of these samples.
All informed consent and research procedures were carried out in accordance to the ethical and regulatory framework set forth by the Ministry of Science and Technology and the Ministry of Health of the People's Republic of China. They have also been approved by the Ethics Committee of the Reproductive Medicine and Prenatal Diagnosis of the 6th Affiliated Hospital of Sun Yat-sen University, and the Ethics Committee of Institute of Zoology, Chinese Academy of Sciences.

Note that full information on the approval of the study protocol must also be provided in the manuscript.